Targeting of Antigen to Dendritic Cells with Poly(γ-Glutamic Acid) Nanoparticles Induces Antigen-Specific Humoral and Cellular Immunity[1]

Tomofumi Uto,*¶ Xin Wang,*¶ Katsuaki Sato,† Misako Haraguchi,‡ Takami Akagi,§¶ Mitsuru Akashi,§¶ and Masanori Baba[2]*¶

Nanoparticles are considered to be efficient tools for inducing potent immune responses by an Ag carrier. In this study, we examined the effect of Ag-carrying biodegradable poly(γ-glutamic acid) (γ-PGA) nanoparticles (NPs) on the induction of immune responses in mice. The NPs were efficiently taken up by dendritic cells (DCs) and subsequently localized in the lysosomal compartments. γ-PGA NPs strongly induced cytokine production, up-regulation of costimulatory molecules, and the enhancement of T cell stimulatory capacity in DCs. These maturational changes of DCs involved the MyD88-mediated NF-κB signaling pathway. In vivo, γ-PGA NPs were preferentially internalized by APCs (DCs and macrophages) and induced the production of IL-12p40 and IL-6. The immunization of mice with OVA-carrying NPs induced Ag-specific CTL activity and Ag-specific production of IFN-γ in splenocytes as well as potent production of Ag-specific IgG1 and IgG2a Abs in serum. Furthermore, immunization with NPs carrying a $CD8^+$ T cell epitope peptide of *Listeria monocytogenes* significantly protected the infected mice from death. These results suggest that Ag-carrying γ-PGA NPs are capable of inducing strong cellular and humoral immune responses and might be potentially useful as effective vaccine adjuvants for the therapy of infectious diseases. *The Journal of Immunology,* 2007, 178: 2979–2986.

The generation of robust and specific immune responses against infectious diseases is a primary goal of vaccination. Novel vaccine candidates being developed are capable of inducing both cellular and humoral immune responses (1, 2). For instance, vaccines against intracellular pathogens such as HIV type 1 and malaria are required to induce strong cellular immune responses, whereas vaccines targeting extracellular microorganisms have to induce humoral immune responses (3–7).

Almost 70 years ago, Freund and colleagues developed the highly potent adjuvant CFA, which is an emulsion of water and mineral oil containing killed mycobacteria (8). Despite a potent activity, CFA also induces severe local reactions and thus cannot be used for humans. Therefore, it seems mandatory to develop less toxic and more effective vaccine adjuvants. Aluminum-based compounds such as aluminum phosphate or hydroxide are safe and currently used as predominant adjuvants in humans. These compounds are able to induce Th2 responses, yet they have little capacity to stimulate Th1 immune responses (9).

Dendritic cells (DCs),[3] the most potent APCs, are defined by their dendritic morphology and unique phenotype. DCs consist of heterogeneous subsets with myeloid or lymphoid lineage as well as different levels of maturity in both lymphoid and peripheral tissues (10). Immature DCs (iDCs) sense the presence of invading pathogens via various pattern-recognition receptors and process the intracellular pathogens in inflammatory tissues. iDCs develop into mature DCs (mDCs) with the up-regulation of MHC and costimulatory molecules in inflammatory microenvironments (10–14). Subsequently, mDCs migrate to secondary lymphoid tissues where they present the processed Ags to naive T cells to effectively generate effector T cells (10). Therefore, the targeting of Ags to DCs is believed to be a promising strategy for the potent and efficient induction of Ag-specific protective immune responses (15–17).

Nanoparticles (NPs) are considered to be efficient Ag carriers and are widely investigated for their biological potential (18, 19). We have previously reported that Con A-immobilized polystyrene NPs could efficiently capture HIV-1 particles and gp120 Ags (20). Immunization with inactivated HIV-1-capturing NPs induced HIV-1-specific IgA Abs in the genital tract of mice (21, 22). Furthermore, intranasal immunization of mice with simian/HIV-capturing NPs could induce mucosal immune responses in macaques, and the macaques immunized with simian/HIV-NPs exhibited partial protection against vaginal and systemic challenge with the virus (23). However, because polystyrene is not biodegradable, it may not be applicable to the clinical situation as a vaccine material

*Division of Antiviral Chemotherapy, Center for Chronic Viral Diseases, Graduate School of Medical and Dental Sciences, Kagoshima University, Kagoshima, Japan; †Laboratory for Dendritic Cell Immunology, Research Center for Allergy and Immunology, Institute of Physical and Chemical Research (Japan), Yokohama Institute, Kanagawa, Japan; ‡Department of Biochemistry and Molecular Biology, Graduate School of Medical and Dental Sciences, Kagoshima University, Kagoshima, Japan; §Department of Molecular Chemistry, Graduate School of Engineering, Osaka University, Osaka, Japan; ¶Core Research for Evolutional Science and Technology (CREST), the Japan Science and Technology Agency (JST), Tokyo, Japan

Received for publication September 8, 2006. Accepted for publication December 22, 2006.

The costs of publication of this article were defrayed in part by the payment of page charges. This article must therefore be hereby marked *advertisement* in accordance with 18 U.S.C. Section 1734 solely to indicate this fact.

[1] This work was supported by Core Research for Evolutional Science and Technology from the Japan Science and Technology Agency.

[2] Address correspondence and reprint requests to Dr. Masanori Baba, Division of Antiviral Chemotherapy, Center for Chronic Viral Diseases, Graduate School of Medical and Dental Sciences, Kagoshima University, 8-35-1 Sakuragaoka, Kagoshima, Japan. E-mail address: m-baba@vanilla.ocn.ne.jp

[3] Abbreviations used in this paper: DC, dendritic cell; FITC-NP, FITC-labeled γ-PGA NP; FITC-OVA, FITC-conjugated OVA; FITC-OVA-NP, FITC-OVA-encapsulating NP; iDC, immature DC; LLO, listerolysin; mDC, mature DC; NP, nanoparticle; OVA-NP, OVA-carrying NP; γ-PGA, poly(γ-glutamic acid).

due to safety reasons. To improve the NP-based vaccine formation, we have successfully generated biodegradable NPs using poly(γ-glutamic acid) (γ-PGA) (24). γ-PGA is a capsular exopolymer produced by certain strains of bacteria. γ-PGA NPs are degraded by γ-glutamyl transpeptidase, which is widely distributed in the whole body. In addition, various molecules such as proteins and peptides can be immobilized on the surface and/or the inside of the particles. In this study, we examined the effect of γ-PGA NPs on DC functions and the efficacy of Ag-carrying γ-PGA NPs for the induction of Ag-specific immune responses.

Materials and Methods

Mice

Female C57BL/6 (H-2K^b, 6–8 wk of age) mice were purchased from Charles River. Experiments were approved by Kagoshima University and conducted in accordance with its guideline for animal experimentation.

Cells

B cells were obtained by the positive selection of splenic mononuclear cells from normal C57BL/6 mice using mAbs to B-220 (BD Biosciences) and sheep anti-rat IgG Ab-conjugated immunomagnetic beads (Dynal Biotech). Macrophages were obtained from peritoneal exudates in C57BL/6 mice injected with 100 μl of 1% thioglycolate. iDCs were prepared by culturing murine bone marrow cells in the presence of 20 ng/ml GM-CSF (PeproTech) for 7 days (25–27). mDCs were obtained from iDCs by cultivation with 1 μg/ml LPS (Sigma-Aldrich) for 2 days.

Nanoparticles

The synthetic procedures for γ-PGA NPs and OVA-carrying γ-PGA NPs (OVA-NPs) have been described in our previous report (28). FITC-labeled γ-PGA NPs (FITC-NPs) were synthesized as follows. γ-PGA was conjugated with L-phenylalanine ethylester and 5-aminoacetamido FITC (Molecular Probes) in the presence of water-soluble carbodiimide. The amount of incorporated FITC was measured by spectrofluorometer. γ-PGA NPs either immobilize or encapsulate the K^b-restricted CD8$^+$ T cell epitope listerolysin (LLO) peptide 296–307 (VAYGRQVYLKLS). LLO-immobilizing NPs were synthesized as follows. A carboxyl group of γ-PGA NPs (10 mg/ml) was activated by water-soluble carbodiimide (1 mg/ml in 20 mM phosphate buffer (pH 5.8)) for 20 min. The activated NPs (5 mg), collected by centrifugation (14,000 × *g* for 15 min), were mixed with 1 ml of the peptide (0.25 mg/ml) in PBS, and the mixture was incubated at 4°C for 24 h. After the reaction, the NPs were centrifuged, washed twice with water, and resuspended at 10 mg/ml in PBS. The amount of peptide was measured by the Lowry method, in which LLO-immobilizing or -encapsulating NPs were added to the same volume of 4% SDS to dissolve the γ-PGA NPs, and the peptide content was determined. One milligram of γ-PGA NPs contained 200 μg of the peptide. The contamination of bacterial endotoxin in γ-PGA NPs was determined by a *Limulus* amoebocyte lysate assay (Seikagaku) and found to be <10 endotoxin units/ml.

Uptake of γ-PGA NPs by APCs in vitro

B cells, macrophages, and iDCs (5 × 10^5 cells per 500 μl) were incubated with 100 μg/ml FITC-NPs for 30 min at 37°C and washed with PBS. The cell-associated fluorescence was measured by FACS (FACSCalibur; BD Biosciences). Cytometric data were analyzed by CellQuestPro (BD Biosciences). To determine intracellular NPs, iDCs were incubated with 10 μg/ml FITC-NPs for 30 min at 37°C and washed with PBS. The cell membrane was labeled with PE-conjugated anti-CD11c for 30 min on ice. The cells were washed twice with PBS and transferred to a 24-well glass-bottom culture plate (Asahi Techno Glass). The cells were fixed with 4% paraformaldehyde in PBS for 10 min at room temperature, washed twice with PBS, and subjected to analysis for intracellular localization of NPs by confocal laser scanning microscopy (LSM5 Pascal: Carl Zeiss). To analyze the intracellular localization of NPs, the lysosomes of iDCs were visualized with 50 nM LysoTracker Red DND-99 (Molecular Probes) for 30 min at 37°C. After washing, the cells were incubated with 10 μg/ml FITC-NPs for 30 min at 37°C. The cells were washed, fixed, and examined by confocal laser scanning microscopy as described above. To investigate the dose and time dependency of NP uptake by iDCs, the cells were incubated in the presence of various concentrations of FITC-NPs (1.5–100 μg/ml) at 37°C. The uptake of FITC-NPs at a fixed concentration (100 μg/ml) was examined at different incubation periods. After washing the cells, the cell-associated fluorescence was measured by FACS. To determine the uptake of FITC-conjugated OVA (FITC-OVA) or FITC-OVA-encapsulating NPs (FITC-OVA-NPs) by iDCs, the cells were incubated with FITC-OVA (25, 50, and 100 μg/ml) or FITC-OVA-NPs (carrying 25, 50, and 100 μg/ml FITC-OVA) for 30 min at 37°C. After washing the cells, the cell-associated fluorescence was measured by FACS.

Analysis for DC activation

To determine cytokine production, iDC (2.5 × 10^5 cells/ml) were stimulated with various concentrations of γ-PGA NPs or 1 μg/ml LPS. At 2, 6, 24, and 48 h after stimulation, culture supernatants were collected and measured for their IL-12p40 and TNF-α levels by ELISA kits (BioSource International). For phenotypic analysis, iDCs were stimulated with various concentrations of γ-PGA NPs or LPS for 48 h. The cells were washed with PBS, stained with a PE-conjugated anti-CD40 mAb (BD Biosciences) for 30 min at 4°C, and subjected to FACS analysis.

Allogeneic MLR

iDCs were stimulated with various concentrations of γ-PGA NPs, CpG oligodeoxynucleotides (InvivoGen), polyinosinic-polycytidylic acid (InvivoGen), or LPS for 48 h. The cells were collected and washed with PBS. T cells were obtained by the negative selection of splenic mononuclear cells obtained from normal BALB/c mice using mAbs to Ly-76, B-220, Ly-6G, and I-A/I-E (BD Biosciences) and sheep anti-rat IgG Ab-conjugated immunomagnetic beads. T cells and DCs were incubated at a ratio of 10:1 in a flat-bottom 96-well plate. After a 4-day incubation, 1 μCi (0.037 MBq) of [^{3}H]thymidine was added to each well. The cells were harvested after 16 h and examined for their radioactivity by liquid scintillation spectroscopy.

Analysis of activation signaling pathway

iDCs (2.5 × 10^5 cells/ml) were preincubated with various concentrations of either the p38 MAPK inhibitor SC68376, the JNK inhibitor SP600125, an ERK inhibitor peptide, or the NF-κB inhibitor parthenolide for 1 h (all from Calbiochem) (29–31). The cells were also preincubated with a MyD88 inhibitor peptide (IMGENEX) for 24 h (32). After incubation, the cells were stimulated with 300 μg/ml γ-PGA NPs or 1 μg/ml LPS for 16 h. Culture supernatants were collected for the determination of their TNF-α levels with an ELISA kit (BioSource International). For NF-κB activation analysis, iDCs (1.25 × 10^5 cells/ml) were stimulated with 300 μg/ml γ-PGA NPs or 1 μg/ml LPS for 2 h. The cells were fixed with 3.7% paraformaldehyde and permeabilized with 0.2% Triton X-100 for 5 min. Then, the cells were stained with a rabbit anti-NF-κB p65 polyclonal Ab for 60 min followed by a FITC-conjugated goat anti-rabbit IgG Ab (both from Santa Cruz Biotechnology) for 60 min at room temperature and subjected to confocal laser scanning microscopy.

Uptake of γ-PGA NPs by APCs in vivo

To examine the uptake of γ-PGA NPs by APCs, including DCs in vivo, FITC-NPs (2.7 mg in 500 μl of PBS) or PBS alone were injected i.v. to mice. After 4 h, spleen cells were collected from the mice and stained with either PE-conjugated anti-CD3 (for T cells), B220 (for B cells), CD11c (for DCs), or F4/80 (for macrophages) mAb and an allophycocyanin-conjugated anti-CD8a (for CD8a$^+$CD11c$^+$ DCs) mAb (all from BD Biosciences) for 30 min at 4°C. The cells were analyzed by FACS. The maturation of spleen DCs was assessed by the following procedures. γ-PGA NPs (5 mg/ml in PBS) or PBS alone were injected i.p. to mice. Their spleens were collected at 20, 40, and 64 h after injection, dissociated into single-cell suspensions, and stained with PE-conjugated anti-CD11c mAb and either FITC-conjugated anti-CD40, anti-CD80, or anti-CD86 mAb. The cells were also analyzed by FACS. For the detection of cytokine production in vivo, γ-PGA NPs (5 mg/ml in PBS) or PBS alone was injected i.p. to mice. At 4 h after injection, the serum levels of IL-12p40 and IL-6 were measured by ELISA.

Immunization of mice with OVA-carrying γ-PGA-NPs

Mice (3–5 mice in each group) were immunized with either PBS, OVA alone (100 μg), CFA plus OVA (100 μg of OVA in CFA), or OVA-NPs (1 mg of NPs carrying 100 μg of OVA) by a rear footpad route on days 0 and 7. On day 14 after the final immunization, spleen cells were collected and cultured with 10 μg/ml K^b-restricted CTL epitope peptide 257–264 of OVA ($OVA_{257-264}$) and 10 U/ml murine rIL-2 (PeproTech) for 5 days. The cells were served as effector cells to examine their OVA-specific CTL activity. EL4 (H-2K^b) cells untreated and treated with the $OVA_{257-264}$ peptide for 16 h were used as the control and target cells, respectively. The cells were labeled with 100 μCi/ml $Na_2[^{51}Cr]O_4$, mixed with the effector

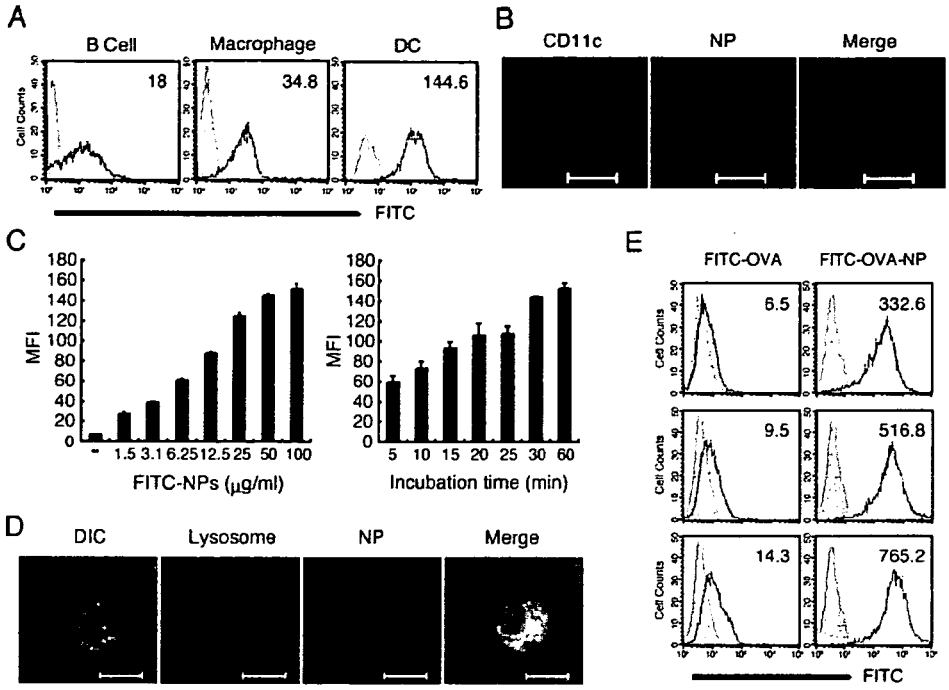

FIGURE 1. Uptake of FITC-γ-PGA NPs by iDCs in vitro. *A*, B cells, macrophages and iDCs were cultured in the presence of FITC-NPs for 30 min at 37°C and cell-associated fluorescence was assessed by flow cytometry. The number in each histogram indicates mean fluorescence intensity of the cells. *B*, iDCs were cultured in the presence of FITC-NPs (green) for 30 min at 37°C and then stained with a PE-conjugated anti-CD11c mAb (red) on ice. Intracellular localization of FITC-γ-PGA NPs was determined by confocal laser scanning microscopy. Bars indicate 10 μm. *C*, iDCs were cultured with the indicated concentrations of FITC-NPs for 60 min at 37°C or cultured with 100 μg/ml FITC-NPs for the indicated time periods at 37°C, and cell-associated fluorescence was assessed by flow cytometry. The experiment was performed in duplicate and results are expressed as mean fluorescence intensity (MFI) ± SD. The results are a representative of three separate experiments. *D*, iDCs were stained with LysoTracker Red DND-99 (red) and cultured in the presence of FITC-PGA NPs (green). Localization of lysosomes and FITC-NPs was determined by confocal laser scanning microscopy. Bars indicate 10 μm. DIC, differential interference contrast. *E*, iDCs were cultured in the presence of FITC-OVA or FITC-OVA-NPs for 30 min at 37°C, and cell-associated fluorescence was assessed by flow cytometry. FITC-OVA concentrations were 25, 50, and 100 μg/ml in *upper*, *middle*, and *lower panels*, respectively.

cells at various effector/target ratios, and further incubated for 4 h. Ag-specific lysis of the target cells was monitored by a standard ^{51}Cr-releasing method as previously described (26).

IFN-γ-producing cells were evaluated by ELISPOT with a mouse IFN-γ ELISPOT kit (BD Biosciences). The collected spleen cells (1×10^6 cells/ml) were restimulated with 10 μg/ml OVA or the $OVA_{257-264}$ peptide in a 96-well ELISPOT plate. The plate was incubated at 37°C for 18 h, washed, and further incubated with a biotin-conjugated detection Ab for 2 h at room temperature. After washing, the plate was incubated with streptavidin-conjugated HRP and incubated for 1 h. The plate was washed again and incubated with the substrate for 15 min. The colorimetric reaction was terminated by washing with water. After drying the plate, the number of spots was counted microscopically.

Serum samples were also collected from the mice on day 14 after the final immunization and subjected to measurement of their anti-OVA Ab titers by ELISA. Briefly, a 96-well plate was coated with OVA suspension in carbonate-bicarbonate buffer (10 μg/ml) and incubated overnight at 4°C. The plate was washed with PBS containing 0.05% Tween 20 (T-PBS) and incubated with 1% BSA and 1% skim milk in T-PBS for 2 h at room temperature. The serum samples serially diluted with T-PBS were added to the wells. After a 2-h incubation at room temperature, the plate was incubated with either alkaline phosphatase-conjugated goat anti-mouse IgG, IgG1, or IgG2a Ab (Southern Biotechnology). The plate was developed by adding the substrate to each well and incubated for 10 min. The colorimetric reaction was terminated by adding a stop solution (2M H_2SO_4), and the absorbance of each well was measured at 450 nm. End point titers were determined by the *x*-axis intercept of the dilution curve.

Listeria monocytogenes *challenge to immunized mice*

Eight mice in each group were immunized with either PBS, LLO peptide alone (100 μg), LLO-immobilizing NPs, or LLO-encapsulating NPs (1 mg of both NPs carrying 10 μg of the peptide) by a rear footpad route on days 0 and 7. On day 14 after the final immunization, the mice were challenged with 5×10^5 of virulent *L. monocytogenes*.

Statistical analysis

Statistical evaluation was performed by Student's *t* test. Statistical analysis for survival of mice was performed with the computer software StatView-J version 5.0.

Results

Uptake of γ-PGA NPs by APCs in vitro

When spleen B cells, peritoneal macrophages, and bone marrow-derived DCs were incubated with FITC-NPs and examined for their NP uptake by flow cytometry, DCs were found to take up FITC-NPs more efficiently than B cells and macrophages (Fig. 1*A*). To determine the intracellular localization γ-PGA NPs, DCs were incubated with FITC-NPs and then labeled with a PE-conjugated anti-CD11c mAb. Green signals inside of the cell membrane clearly showed the uptake of NPs by DCs (Fig. 1*B*). When the dose and time dependency of NP uptake by DCs was examined, the amount of intracellular NPs increased with increasing concentrations and incubation times of NPs, indicating that the uptake was both dose and time dependent (Fig. 1*C*). However, a further increase of incubation time up to 24 h did not significantly increase the amount of intracellular NPs (data not shown). To further determine the intracellular localization of NPs in DCs, lysosomes were stained with a lysosome-specific dye. Internalized NPs were mostly detected along with the lysosomes of DCs (Fig. 1*D*),

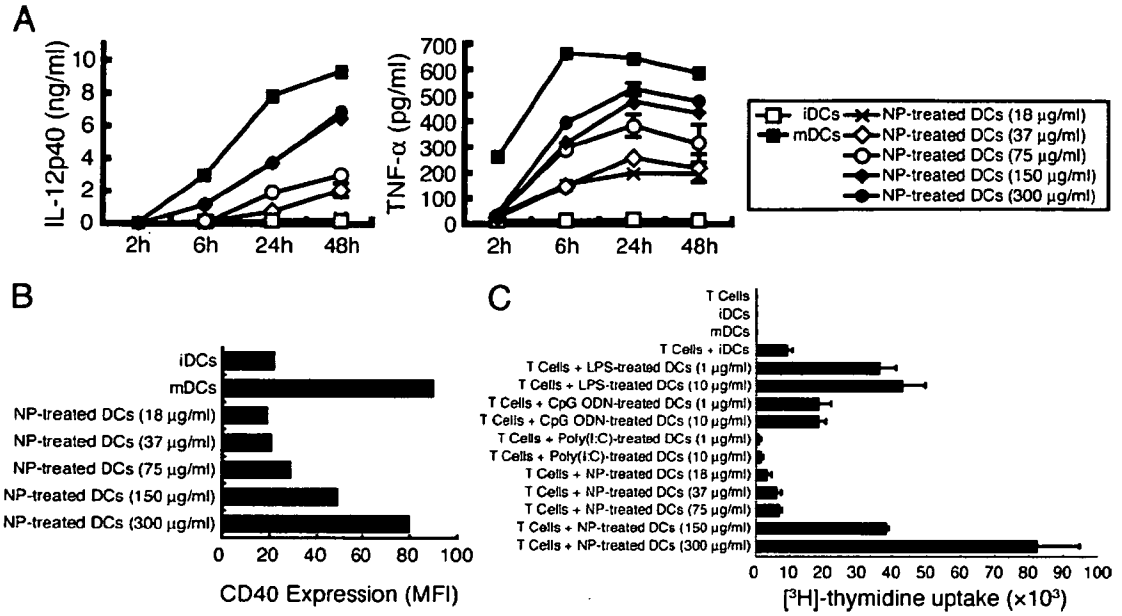

FIGURE 2. Maturation and activation of DCs by γ-PGA NPs. *A*, iDCs were cultured with the indicated concentrations of γ-PGA NPs or 1 μg/ml LPS. Culture supernatants were collected at different time points after cultivation. Cytokine levels were measured by ELISA. The experiment was performed in duplicate, and the results are expressed as means ± ranges. The results are a representative of three separate experiments. *B*, iDCs were cultured in the presence of indicated concentration of γ-PGA NPs or 1 μg/ml LPS. After 2 days the cells were collected, stained with anti-CD11c-PE and anti-CD40-FITC mAbs, and analyzed by flow cytometry. Data are expressed as mean fluorescence intensity (MFI). The results are a representative of three separate experiments. *C*, iDCs were cultured with the indicated concentrations of γ-PGA NPs, CpG oligodeoxynucleotide (ODN), polyinosinic-polycytidylic acid (poly(I:C)), or LPS. After 2 days the cells were collected and cocultured with allogeneic normal T cells for 4 days. Proliferative response was measured by [^{3}H]thymidine uptake on day 5. Data are expressed as mean ± SD. The results are a representative of three separate experiments.

indicating that internalized NPs preferentially localized in the lysosomal compartments. Furthermore, it is clear that the NP-associated form of OVA (FITC-OVA-NPs) could be taken up much more efficiently by DCs than the NP-free form of OVA (FITC-OVA) (Fig. 1*E*). γ-PGA NPs did not affect the viability of DCs after 48 h of cocultivation at concentrations up to 300 μg/ml (data not shown).

Maturation and activation of DCs by γ-PGA NPs

To examine the effect of γ-PGA NPs on DC maturation, iDCs were cultured in the presence of various concentrations of γ-PGA NPs. When cytokine production was examined, iDCs did not produce detectable levels of IL-12p40 and TNF-α. In contrast, both cytokines were abundantly produced from mDCs and NP-treated DCs in dose- and time-dependent fashions (Fig. 2*A*). Furthermore, NP-treated DCs also produced IL-1β and IL-6 (data not shown). The maturation of iDCs is accompanied by the enhanced expression of surface markers, including costimulatory molecules and MHC complexes. Treatment of iDCs with γ-PGA NPs resulted in a marked increase of CD40 expression on their surfaces in a dose-dependent fashion (Fig. 2*B*). CD86, MHC class I, and MHC class II expressions were also up-regulated in NP-exposed DCs, as compared with iDCs (data not shown). Like mDCs, NP-treated DCs showed strong capacity to stimulate allogeneic T cells in a dose-dependent fashion (Fig. 2*C*).

γ-PGA NPs induce NF-κB activation via a MyD88-dependent pathway

To clarify the signaling pathway underlying γ-PGA NP-induced DC maturation, we examined the effect of various inhibitors on γ-PGA NP-induced TNF-α production in DCs. Treatment with the p38 MAPK inhibitor SC68376 suppressed both LPS- and NP-induced TNF-α production, whereas the JNK inhibitor SP600125 failed to do so (Fig. 3*A*). Although an ERK inhibitor peptide did not inhibit NP-induced TNF-α production, it suppressed LPS-induced TNF-α production (Fig. 3*A*). In contrast, a MyD88 inhibitor peptide, but not a control peptide, significantly reduced TNF-α production in both NP- and LPS-treated DCs (Fig. 3*B*). We also examined the nuclear translocation of the p65 subunit of NF-κB by confocal laser scanning microscopy. The p65 subunit was located in the cytoplasm of the untreated cells, whereas the translocation of p65 into the nucleus was detected in both NP- and LPS-treated DCs (Fig. 3*C*). Furthermore, treatment with the NF-κB inhibitor parthenolide showed more profound suppression on TNF-α production in NP-treated DCs than in LPS-treated DCs (Fig. 3*D*).

Uptake of γ-PGA NPs by APCs in vivo

To examine the uptake of γ-PGA NPs in vivo, spleen cells were collected from mice at 4 h after i.v. administration of FITC-NPs. The FITC-positive cells were detectable in B cells, DCs, and macrophages but not in T cells. The number of FTIC-positive cells was the highest in DCs compared with other cell types (Fig. 4*A*). CD8a$^+$ lymphoid DCs play an important role in the initiation of the Th1 cell-biased immune response as well as the cross-presentation of processed Ags to CD8$^+$ T cells, leading to the generation of Ag-specific CTLs (17). To determine whether FITC-NPs are taken up by CD8a$^+$ DCs, the spleen cells were stained with anti-CD11c and anti-CD8 mAbs and examined for their FITC-positive population. Approximately one-third (34.3%) of the FITC-positive cells were CD11c$^+$ DCs, and 3.21% of the FITC-positive cells (9.4% of the CD11c$^+$ DCs) was also CD8a$^+$ (Fig. 4*B*). When CD40, CD80, and CD86 expressions were examined

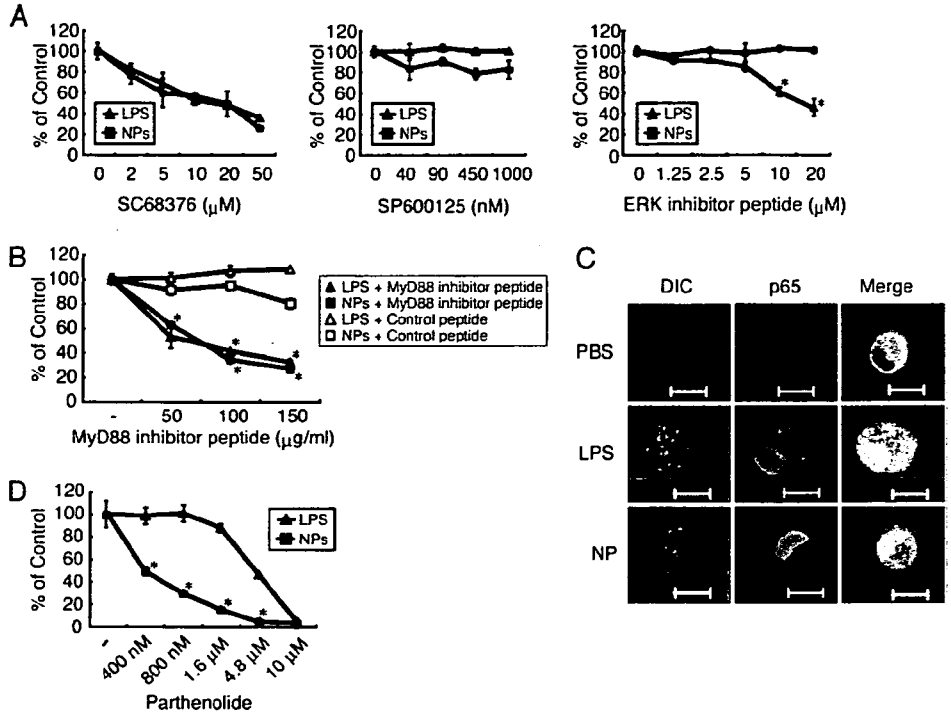

FIGURE 3. Effect of various inhibitors on DC activation by γ-PGA NPs. *A*, iDCs were preincubated with the indicated concentrations of SC68376, SP600125, or an ERK inhibitor peptide for 1 h. After incubation, the cells were stimulated with 300 μg/ml γ-PGA NPs or 1 μg/ml LPS and cultured for 16 h. Culture supernatants were collected and determined for their TNF-α level by ELISA. *B*, iDCs were preincubated with the indicated concentrations of either a MyD88 inhibitor peptide or a control peptide for 1 h. After incubation, the cells were stimulated with 300 μg/ml γ-PGA NPs or 1 μg/ml LPS and cultured for 16 h. Culture supernatants were collected and determined for their TNF-α level by ELISA. *C*, iDCs were stimulated with 300 μg/ml γ-PGA or 1 μg/ml LPS for 2 h. The cells were fixed, permeabilized, and stained with a rabbit anti-NF-κB p65 polyclonal Ab followed by an FITC-conjugated goat anti-rabbit IgG Ab. The localization of p65 was determined by confocal laser scanning microscopy. Bars indicate 10 μm. *D*, iDCs were preincubated with the indicated concentrations of parthenolide. After incubation, the cells were stimulated with 300 μg/ml γ-PGA NPs or 1 μg/ml LPS and cultured for 16 h. Culture supernatants were collected to determine their TNF-α level. Except for the p65 localization experiment, all experiments were performed in triplicate and data are expressed as means ± SD. The results are a representative of three separate experiments. Statistical evaluation for the results was conducted between the corresponding two groups. *, $p < 0.05$.

for spleen DCs obtained from NP-treated mice, the enhanced expression of these molecules was identified most clearly at 40 h after NP-treatment of mice (Fig. 4*C*). However, such enhancement was not observed for PBS-treated mice. The serum IL-12p40 and IL-6 levels were found to be significantly higher in NP-treated mice than in PBS-treated mice (Fig. 4*D*).

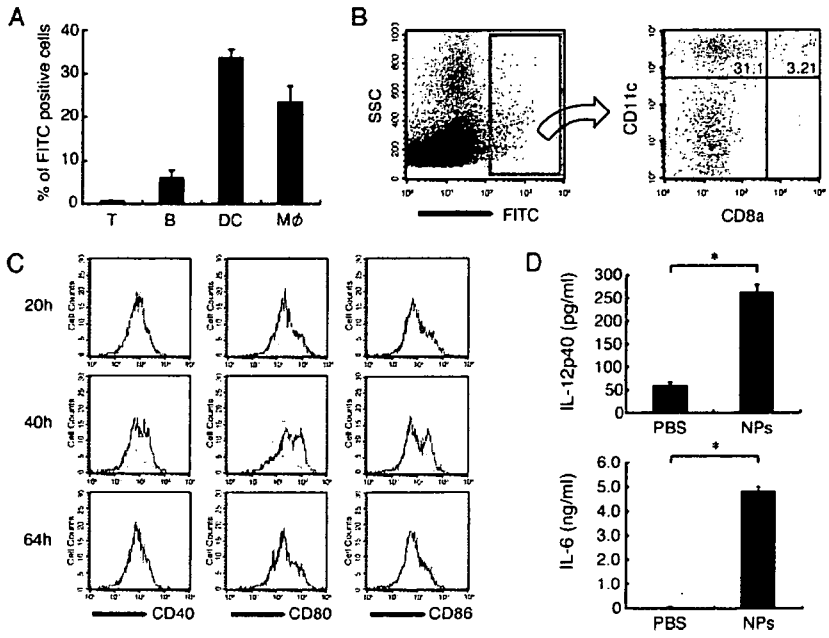

FIGURE 4. Uptake of γ-PGA NPs by DCs and their maturation in vivo. *A*, PBS or 2.7 mg of FITC-NPs were injected into mice through their tail veins. After 4 h, spleen cells (T, T cells; B, B cells; Mϕ, macrophages) were collected, stained with PE-conjugated anti-CD3, anti-B220, anti-CD11c, or anti-F4/80 mAbs, and analyzed by flow cytometry. *B*, PBS or FITC-NPs were injected, as described above. Spleen cells were collected and stained with PE-conjugated anti-CD11c and allophycocyanin-conjugated anti-CD8a mAbs. The FITC-positive cells were analyzed by FACS. The results from a representative experiment among three separate experiments are shown. *C*, PBS or 5 mg of γ-PGA NPs were injected i.p. to mice. At various time points spleen cells were collected, stained with PE-conjugated anti-CD11c and FITC-conjugated anti-CD40, anti-CD80, and anti-CD86 mAbs, and analyzed by flow cytometry. *D*, PBS or 5 mg of γ-PGA NPs were injected i.p. to mice. After 4 h, sera were collected and cytokine levels were measured by ELISA. The experiment was performed in triplicate, and data are expressed as means ± SD. *, $p < 0.05$.

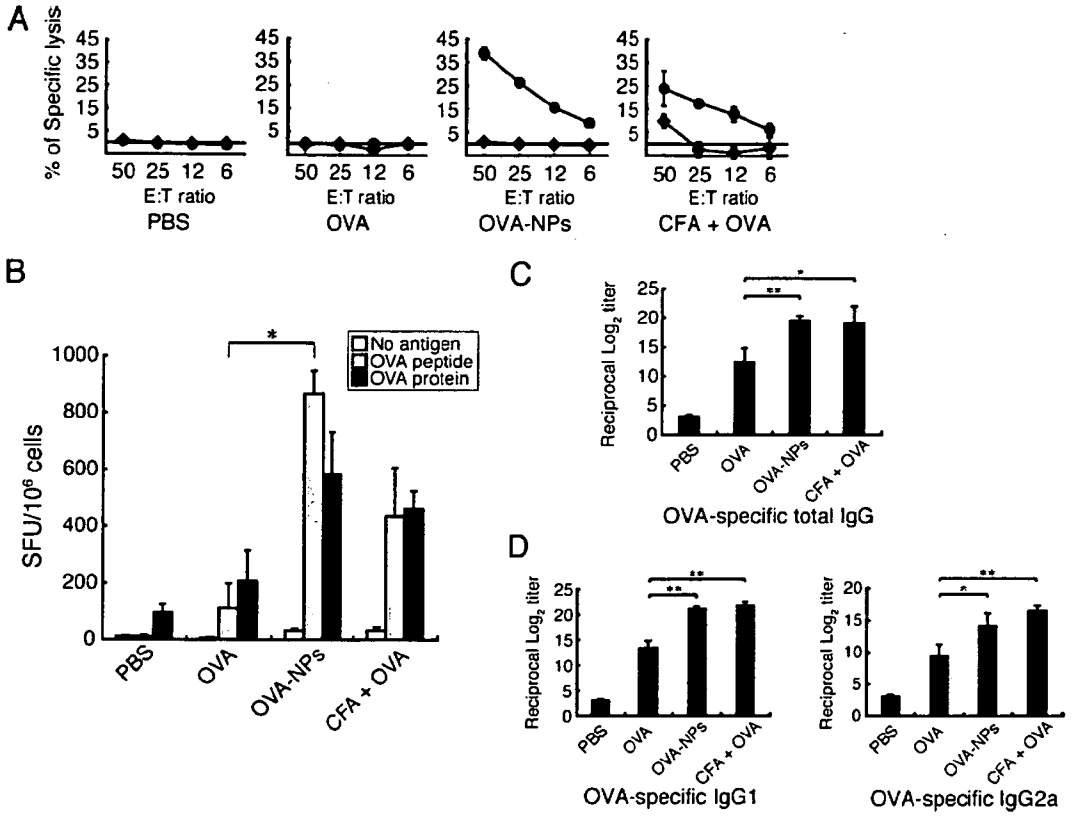

FIGURE 5. Induction of Ag-specific cellular and humoral immune responses by OVA-NPs. Mice were immunized with either PBS, OVA, OVA-NPs, or CFA plus OVA through their footpads. *A*, Spleen cells were restimulated with the $OVA_{257-264}$ peptide and IL-2. The spleen cells were examined for their cytolytic activity to peptide-treated or untreated EL4 target cells at various E:T ratios by a standard ^{51}Cr-releasing assay. The experiments were performed in triplicate, and data are expressed as means ± SD. The results are a representative of three separate experiments. The difference in specific lysis between the OVA-NPs group and the CFA plus OVA group is statistically significant ($p < 0.05$) at an E:T ratio of 50. *B*, Spleen cells were restimulated with the $OVA_{257-264}$ peptide or OVA protein. IFN-γ producing T cells were counted and expressed as the spot forming unit (SFU) per one million cells. Data represent means ± SD for three to four separate experiments. *, $p < 0.05$. *C* and *D*, Sera were tested for their Ab titers of OVA-specific IgG and its subclasses as determined by ELISA. Data represent means ± SD of endpoint titers for three to four separate experiments. *, $p < 0.05$, **, $p < 0.005$.

OVA-carrying γ-PGA NPs induce Ag-specific immune responses

The efficacy of Ag-capturing γ-PGA NPs on the induction of Ag-specific cellular and humoral immune responses was examined using OVA as a model Ag. As shown in Fig. 5*A*, an Ag-specific CTL response was not observed in the spleen cells obtained from the control (PBS) and OVA-immunized mice. In contrast, the spleen cells obtained from the mice immunized with OVA-NPs showed a more potent Ag-specific CTL response than those obtained from mice immunized with OVA plus CFA (Fig. 5*A*). In addition, the number of Ag-specific IFN-γ producing cells was significantly higher in the OVA-NP group than the OVA group (Fig. 5*B*). When a K^b-restricted control peptide was used for stimulation, no such induction of IFN-γ producing cells was identified (data not shown). Furthermore, a similar level of cellular immune responses was observed in mice immunized with reduced doses of OVA-NPs (data not shown). When Ag-specific Ab responses were examined and compared among the groups after immunization, both OVA-NP- and (OVA plus CFA)-immunized mice showed significantly higher levels of OVA-specific total IgG, IgG1, and IgG2a Abs than OVA-immunized mice (Fig. 5, *C* and *D*).

Protection of mice from L. monocytogenes *infection*

Challenge with a lethal dose of live bacteria is a stringent test for the efficacy of vaccination. *L. monocytogenes* infection in mice seems to be a representative model for evaluating $CD8^+$ T cell-mediated protection against intracellular pathogens (33–35). Fourteen days after the final immunization the mice were infected with a lethal dose of viable *L. monocytogenes* and monitored daily for their survival. Approximately 80% of the mice immunized with

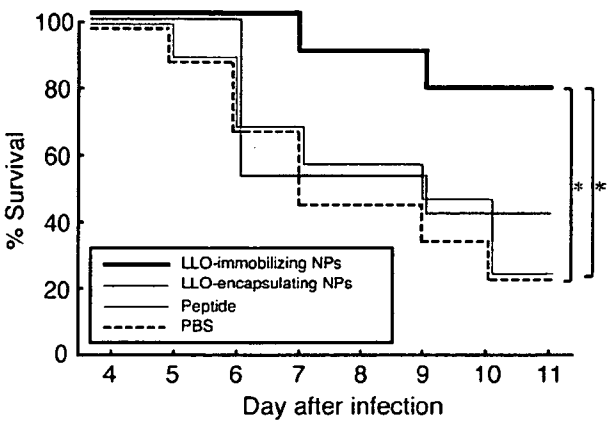

FIGURE 6. Protection of mice from *L. monocytogenes* infection. Mice (8 mice in each group) were immunized with either PBS (dotted line), LLO peptide alone (solid line), LLO-immobilizing NPs (heavy line), or LLO-encapsulating NPs (gray line) by a rear footpad route on days 0 and 7. On day 14 after the final immunization, the mice were infected with a lethal dose of *L. monocytogenes*. Survival of mice after infection was monitored up to 11 days. *, $p < 0.05$.

LLO-immobilizing NPs had survived by day 11 after infection. In contrast, most of the control mice and those immunized with the LLO peptide alone succumbed to the infection (Fig. 6). Little if any protection was observed for the mice immunized with LLO-encapsulating NPs. These results indicate that immunization with LLO-immobilizing NPs was efficient in protecting the mice from lethal infection with *L. monocytogenes*.

Discussion

Several attempts have been made to identify the strategies that induce potent immunostimulatory activities (36–38). However, most of the experimental adjuvants cannot be used for humans due to their side effects. At present, only the aluminum salt alum has been approved for clinical use, yet it has only weak activity. We have recently created biodegradable γ-PGA NPs that have potent immunomodulatory activities as well as an excellent capacity of carrying various proteins and peptides.

In this study, we showed that γ-PGA NPs were taken up by DCs most efficiently than by other APCs, such as macrophages and B cells, and localized in the lysosomes (Fig. 1). Although the mechanism of NP uptake remains to be elucidated, phagocytosis inhibitors showed modest (~30%) inhibition of the uptake by DCs (data not shown). It has been demonstrated that exogenous peptides can be acquired for cross-presentation to T cells through the MHC class I in the endolysosomal compartment of DCs (39). Analysis of the functional properties of DCs revealed that γ-PGA NPs were able to strongly induce DC activation. Activation of DCs through CD40 and IL-12p40 signaling pathways were needed for linkage between innate and adaptive immunity, including $CD4^+$ and $CD8^+$ T cell responses to DCs (40). In fact, NP-treated DCs could induce the production of the innate inflammatory cytokines IL-12p40 and TNF-α as well as CD40 expression and the strong stimulation of allogeneic T cells (Fig. 2). These results suggest that γ-PGA NPs are capable of inducing both innate and adaptive immunity through DC activation.

Analysis of the signaling pathway in NP-treated DCs indicated the involvement of MyD88-mediated NF-κB activation and p38 MAPK (Fig. 3). Similar results were also obtained with LPS-treated DCs. However, the ERK inhibitor could suppress TNF-α production in LPS-treated DCs but not in NP-treated DCs. Furthermore, the NF-κB inhibitor parthenolide was found to more effectively suppress TNF-α production in NP-treated DCs than in LPS-treated DCs. Thus, it appears that the signaling pathway involved in NP stimulation overlaps but is not identical with the pathway involved in LPS-stimulation. Presumably, fewer numbers of signal transduction molecules may participate in NP-induced NF-κB activation than in LPS-induced NF-κB activation. It is also noteworthy that unparticulated γ-PGA did not have sufficient activity to induce DC maturation (data not shown), indicating that the nanoparticle form of γ-PGA is required to interact with a certain molecule necessary for DC activation. Further studies are in progress to determine whether γ-PGA NPs interact with TLRs.

Because γ-PGA NPs proved to be predominantly taken up into spleen DCs and could up-regulate the expression of costimulatory molecules in vivo (Fig. 4), the γ-PGA NPs seem to be a promising candidate for a vaccine adjuvant. The uptake of Ags by DCs results in their subsequent migration to lymph nodes, increased production of cytokines, and enhanced expression of costimulatory and MHC molecules followed by Ag presentation to T cells. In mice DCs are divided into three subclasses, $CD11c^+CD8a^+CD4^-$, $CD11c^+CD8a^-CD4^-$, and $CD11c^+CD8a^-CD4^+$ (41). $CD8a^+$ DCs have been shown to play an important role in cross-priming to $CD8^+$ T cells (42, 43). Indeed, γ-PGA NPs were found to be taken up by $CD8a^+$ DCs, which may directly activate T cells in vivo.

OVA-NPs strongly induced OVA-specific IFN-γ producing cells, CTL activity, and Ab production (Fig. 5). These results suggest that potent cellular and humoral immune responses can be generated by γ-PGA NPs carrying not only OVA but also other peptides or proteins. In fact, γ-PGA NPs carrying HIV-1 Ags were found to induce strong Ag-specific cellular and humoral immunity in mice (X. Wang, T. Uto, T. Akagi, M. Akashi, and M. Baba, manuscript in preparation). Another remarkable observation is that LLO-immobilizing NPs could protect the immunized mice from lethal infection with the intracellular bacterium *L. monocytogenes* (Fig. 6). Taken together, γ-PGA NPs have great potential not only as efficient vaccine carriers but also as effective adjuvants in vivo.

In conclusion, the present study clearly shows the effectiveness of the γ-PGA NP as an Ag delivery system and an adjuvant to DCs in vitro and in vivo. Further studies, including the optimization of γ-PGA NPs and immunization with Ag-carrying NPs in other animal species, are in progress for the clinical development of this novel vaccine candidate.

Acknowledgment

We thank Dr. C. Koriyama for excellent advice on statistical evaluation in mouse experiments.

Disclosures

M. A. and M. B. are applying for a patent on nanoparticles. All other authors have no financial conflicts of interest.

References

1. Hutchings, C. L., S. C. Gilbert, A. V. Hill, and A. C. Moore. 2005. Novel protein and poxvirus-based vaccine combinations for simultaneous induction of humoral and cell-mediated immunity. *J. Immunol.* 175: 599–606.
2. Tritel, M., A. M. Stoddard, B. J. Flynn, P. A. Darrah, C. Y. Wu, U. Wille, J. A. Shah, Y. Huang, L. Xu, M. R. Betts, et al. 2003. Prime-boost vaccination with HIV-1 Gag protein and cytosine phosphate guanosine oligodeoxynucleotide, followed by adenovirus, induces sustained and robust humoral and cellular immune responses. *J. Immunol.* 171: 2538–2547.
3. Hanke, T., A. J. McMichael, M. Mwau, E. G. Wee, I. Ceberej, S. Patel, J. Sutton, M. Tomlinson, and R. V. Samuel. 1998. Development of a DNA-MVA/HIVA vaccine for Kenya. *Vaccine* 20: 1995–1998.
4. Moore, A. C., and A. V. Hill. 2004. Progress in DNA-based heterologous prime-boost immunization strategies for malaria. *Immunol. Rev.* 199: 126–143.
5. Schneider, J., S. C. Gilbert, T. J. Blanchard, T. Hanke, K. J. Robson, C. M. Hannan, M. Becker, R. Sinden, G. L. Smith, and A. V. Hill. 1998. Enhanced immunogenicity for $CD8^+$ T cell induction and complete protective efficacy of malaria DNA vaccination by boosting with modified vaccinia virus Ankara. *Nat. Med.* 4: 397–402.
6. Letvin, N. L., D. H. Barouch, and D. C. Montefiori. 2002. Prospects for vaccine protection against HIV-1 infection and AIDS. *Annu. Rev. Immunol.* 20: 73–99.
7. Good, M. F., D. C. Kaslow, and L. H. Miller. 1998. Pathways and strategies for developing a malaria blood-stage vaccine. *Annu. Rev. Immunol.* 16: 57–87.
8. Freund, J., J. Casals, and E. P. Hosmer. 1937. Sensitization and antibody formation after injection of tubercle bacili and paraffin oil. *Proc. Soc. Exp. Biol. Med.* 37: 509–513.
9. Petrovsky, N., and J. C. Aguilar. 2004. Vaccine adjuvants: current state and future trends. *Immunol. Cell Biol.* 82: 488–496.
10. Banchereau, J., F. Briere, C. Caux, J. Davoust, S. Lebecque, Y. J. Liu, B. Pulendran, and K. Palucka. 2000. Immunobiology of dendritic cells. *Annu. Rev. Immunol.* 18: 767–811.
11. Krieg, A. M. 2002. CpG motifs in bacterial DNA and their immune effects. *Annu. Rev. Immunol.* 20: 709–760.
12. Iwasaki, A., and R. Medzhitov. 2004. Toll-like receptor control of the adaptive immune responses. *Nat. Immunol.* 5: 987–995.
13. Sparwasser, T., E. S. Koch, R. M. Vabulas, K. Heeg, G. B. Lipford, J. W. Ellwart, and H. Wagner. 1998. Bacterial DNA and immunostimulatory CpG oligonucleotides trigger maturation and activation of murine dendritic cells. *Eur. J. Immunol.* 28: 2045–2054.
14. Lore, K., M. R. Betts, J. M. Brenchley, J. Kuruppu, S. Khojasteh, S. Perfetto, M. Roederer, R. A. Seder, and R. A. Koup. 2003. Toll-like receptor ligands modulate dendritic cells to augment cytomegalovirus- and HIV-1-specific T cell responses. *J. Immunol.* 171: 4320–4328.
15. Badovinac, V. P., K. A. Messingham, A. Jabbari, J. S. Haring, and J. T. Harty. 2005. Accelerated $CD8^+$ T-cell memory and prime-boost response after dendritic-cell vaccination. *Nat. Med.* 11: 748–756.

16. Luci, C., C. Hervouet, D. Rousseau, J. Holmgren, C. Czerkinsky, and F. Anjuere. 2006. Dendritic cell-mediated induction of mucosal cytotoxic responses following intravaginal immunization with the nontoxic B subunit of cholera toxin. *J. Immunol.* 176: 2749–2757.
17. Porgador, A., and E. Gilboa. 1995. Bone marrow-generated dendritic cells pulsed with a class I-restricted peptide are potent inducers of cytotoxic T lymphocytes. *J. Exp. Med.* 182: 255–260.
18. Coester, C., P. Nayyar, and J. Samuel. 2006. In vitro uptake of gelatin nanoparticles by murine dendritic cells and their intracellular localisation. *Eur. J. Pharm. Biopharm.* 62: 306–314.
19. Dinauer, N., S. Balthasar, C. Weber, J. Kreuter, K. Langer, and H. von Briesen. 2005. Selective targeting of antibody-conjugated nanoparticles to leukemic cells and primary T-lymphocytes. *Biomaterials* 26: 5898–5906.
20. Hayakawa, T., M. Kawamura, M. Okamoto, M. Baba, T. Niikawa, S. Takehara, T. Serizawa, and M. Akashi. 1998. Concanavalin A-immobilized polystyrene nanospheres capture HIV-1 virions and gp120: potential approach towards prevention of viral transmission. *J. Med. Virol.* 56: 327–331.
21. Kawamura, M., T. Naito, M. Ueno, T. Akagi, K. Hiraishi, I. Takai, M. Makino, T. Serizawa, K. Sugimura, M. Akashi, and M. Baba. 2002. Induction of mucosal IgA following intravaginal administration of inactivated HIV-1-capturing nanospheres in mice. *J. Med. Virol.* 66: 291–298.
22. Akagi, T., M. Kawamura, M. Ueno, K. Hiraishi, M. Adachi, T. Serizawa, M. Akashi, and M. Baba. 2003. Mucosal immunization with inactivated HIV-1-capturing nanospheres induces a significant HIV-1-specific vaginal antibody response in mice. *J. Med. Virol.* 69: 163–172.
23. Miyake, A., T. Akagi, Y. Enose, M. Ueno, M. Kawamura, R. Horiuchi, K. Hiraishi, M. Adachi, T. Serizawa, O. Narayan, et al. 2004. Induction of HIV-specific antibody response and protection against vaginal SHIV transmission by intranasal immunization with inactivated SHIV-capturing nanospheres in macaques. *J. Med. Virol.* 73: 368–377.
24. Akagi, T., M. Higashi, T. Keneko, T. Kida, and M. Akashi. 2005. In vitro enzymatic degradation of nanoparticles prepared from hydrophobically-modified poly(γ-glutamic acid). *Macromol. Biosci.* 14: 598–602.
25. Wang, X., T. Uto, K. Sato, K. Ide, T. Akagi, M. Okamoto, T. Kaneko, M. Akashi, and M. Baba. 2005. Potent activation of antigen-specific T cells by antigen-loaded nanospheres. *Immunol. Lett.* 98: 123–130.
26. Sato, K., N. Yamashita, N. Yamashita, M. Baba, and T. Matsuyama. 2003. Regulatory dendritic cells protect mice from murine acute graft-versus-host disease and leukemia relapse. *Immunity* 18: 367–379.
27. Sato, K., N. Yamashita, M. Baba, and T. Matsuyama. 2003. Modified myeloid dendritic cells act as regulatory dendritic cells to induce anergic and regulatory T cells. *Blood* 101: 3581–3589.
28. Akagi, T., T. Kaneko, T. Kida, and M. Akashi. 2005. Preparation and characterization of biodegradable nanoparticles based on poly(γ-glutamic acid) with l-phenylalanine as a protein carrier. *J. Controlled Release* 108: 226–236.
29. Bennett, B. L., D. T. Sasaki, B. W. Murray, E. C. O'Leary, S. T. Sakata, W. Xu, J. C. Leisten, A. Motiwala, S. Pierce, Y. Satoh, et al. 2001. SP600125, an anthrapyrazolone inhibitor of Jun N-terminal kinase. *Proc. Natl. Acad. Sci. USA* 98: 13681–13686.
30. Kelemen, B. R., K. Hsiao, and S. A. Goueli. 2002. Selective in vivo inhibition of mitogen-activated protein kinase activation using cell-permeable peptides. *J. Biol. Chem.* 277: 8741–8748.
31. Bork, P. M., M. L. Schmitz, M. Kuhnt, C. Escher, and M. Heinrich. 1997. Sesquiterpene lactone containing Mexican Indian medicinal plants and pure sesquiterpene lactones as potent inhibitors of transcription factor NF-κB. *FEBS Lett.* 402: 85–90.
32. Loiarro, M., C. Sette, G. Gallo, A. Ciacci, N. Fanto, D. Mastroianni, P. Carminati, and V. Ruggiero. 2005. Peptide-mediated interference of TIR domain dimerization in MyD88 inhibits interleukin-1-dependent activation of NF-κB. *J. Biol. Chem.* 280: 15809–15814.
33. Nagata, T., T. Aoshi, M. Suzuki, M. Uchijima, Y. H. Kim, Z. Yang, and Y. Koide. 2002. Induction of protective immunity to *Listeria monocytogenes* by immunization with plasmid DNA expressing a helper T-cell epitope that replaces the class II-associated invariant chain peptide of the invariant chain. *Infect. Immun.* 70: 2676–2680.
34. Suzue, K., T. Asai, T. Takeuchi, and S. Koyasu. 2003. In vivo role of IFN-γ produced by antigen-presenting cells in early host defense against intracellular pathogens. *Eur. J. Immunol.* 33: 2666–2675.
35. Geninat, G., S. Schenk, M. Skoberne, W. Goebel, and H. Hof. 2001. A novel approach of direct ex vivo epitope mapping identifies dominant and subdominant CD4 and CD8 T cell epitopes from *Listeria monocytogenes*. *J. Immunol.* 166: 1877–1884.
36. Wan, T., X. Zhou, G. Chen, H. An, T. Chen, W. Zhang, S. Liu, Y. Jiang, F. Yang, Y. Wu, and X. Cao. 2004. Novel heat shock protein Hsp70L1 activates dendritic cells and acts as a Th1 polarizing adjuvant. *Blood* 103: 1747–1754.
37. Wille-Reece, U., C. Y. Wu, B. J. Flynn, R. M. Kedl, and R. A. Seder. 2005. Immunization with HIV-1 Gag protein conjugated to a TLR7/8 agonist results in the generation of HIV-1 Gag-specific Th1 and $CD8^+$ T cell responses. *J. Immunol.* 174: 7676–7683.
38. Becker, P. D., S. Fiorentini, C. Link, G. Tosti, T. Ebensen, A. Caruso, and C. A. Guzman. 2006. The HIV-1 matrix protein p17 can be efficiently delivered by intranasal route in mice using the TLR 2/6 agonist MALP-2 as mucosal adjuvant. *Vaccine* 24: 5269–5276.
39. Lizee, G., G. Basha, J. Tiong, J. P. Julien, M. Tian, K. E. Biron, and W. A. Jefferies. 2003. Control of dendritic cell cross-presentation by the major histocompatibility complex class I cytoplasmic domain. *Nat. Immunol.* 4: 1065–1073.
40. Fujii, S., K. Liu, C. Smith, A. J. Bonito, and R. M. Steinman. 2004. The linkage of innate to adaptive immunity via maturing dendritic cells in vivo requires CD40 ligation in addition to antigen presentation and CD80/86 costimulation. *J. Exp. Med.* 199: 1607–1618.
41. Manickasingham, S. P., A. D. Edwards, O. Schulz, and C. Reis e Sousa. 2003. The ability of murine dendritic cell subsets to direct T helper cell differentiation is dependent on microbial signals. *Eur. J. Immunol.* 33: 101–107.
42. Den Haan, J. M., S. M. Lehar, and M. J. Bevan. 2000. $CD8^+$ but not $CD8^-$ dendritic cells cross-prime cytotoxic T cells in vivo. *J. Exp. Med.* 192: 1685–1696.
43. Maldonado-Lopez, R., T. De Smedt, P. Michel, J. Godfroid, B. Pajak, C. Heirman, K. Thielemans, O. Leo, J. Urbaim, and M. Moser. 1999. $CD8\alpha^+$ and $CD8\alpha^-$ subclasses of dendritic cells direct the development of distinct T helper cells in vivo. *J. Exp. Med.* 189: 587–592.

JOURNAL OF VIROLOGY, Sept. 2007, p. 10009–10016 Vol. 81, No. 18
0022-538X/07/$08.00+0 doi:10.1128/JVI.00489-07

Induction of Potent CD8$^+$ T-Cell Responses by Novel Biodegradable Nanoparticles Carrying Human Immunodeficiency Virus Type 1 gp120$^\nabla$

Xin Wang,[1,3] Tomofumi Uto,[1,3] Takami Akagi,[2,3] Mitsuru Akashi,[2,3] and Masanori Baba[1,3]*

Division of Antiviral Chemotherapy, Center for Chronic Viral Diseases, Graduate School of Medical and Dental Sciences, Kagoshima University, Kagoshima 890-8544,[1] Department of Applied Chemistry, Graduate School of Engineering, Osaka University, Suita 565-0871,[2] and Core Research for Evolutional Science and Technology (CREST), Japan Science and Technology Agency (JST), Tokyo 150-0002,[3] Japan

Received 8 March 2007/Accepted 27 June 2007

The mainstream of recent anti-AIDS vaccines is a prime/boost approach with multiple doses of the target DNA of human immunodeficiency virus type 1 (HIV-1) and recombinant viral vectors. In this study, we have attempted to construct an efficient protein-based vaccine using biodegradable poly(γ-glutamic acid) (γ-PGA) nanoparticles (NPs), which are capable of inducing potent cellular immunity. A significant expansion of CD8$^+$ T cells specific to the major histocompatibility complex class I-restricted gp120 epitope was observed in mice intranasally immunized once with gp120-carrying NPs but not with gp120 alone or gp120 together with the B-subunit of cholera toxin. Both the gp120-encapsulating and -immobilizing forms of NPs could induce antigen-specific spleen CD8$^+$ T cells having a functional profile of cytotoxic T lymphocytes. Long-lived memory CD8$^+$ T cells could also be elicited. Although a substantial decay in the effector memory T cells was observed over time in the immunized mice, the central memory T cells remained relatively constant from day 30 to day 238 after immunization. Furthermore, the memory CD8$^+$ T cells rapidly expanded with boosting with the same immunogen. In addition, γ-PGA NPs were found to be a much stronger inducer of antigen-specific CD8$^+$ T-cell responses than nonbiodegradable polystyrene NPs. Thus, γ-PGA NPs carrying various HIV-1 antigens may have great potential as a novel priming and/or boosting tool in current vaccination regimens for the induction of cellular immune responses.

The development of highly active antiretroviral therapy has achieved a reduced death rate from human immunodeficiency virus type 1 (HIV-1) infection in developed countries. However, considering the high cost and potential toxicity of long-term highly active antiretroviral therapy, it is obvious that the development of vaccines against HIV-1 is the most desirable option for the prevention of viral transmission and disease progression (12, 14). An effective anti-AIDS vaccine will likely need to induce virus-specific neutralizing antibodies and cytotoxic T-lymphocyte (CTL) responses. Although neutralizing antibodies have shown the activity to block HIV-1 and simian immunodeficiency virus (SIV), an immunogen inducing the antibodies that neutralize a diversity of primary HIV-1 isolates has not been obtained. With accumulating evidence for the importance of CTLs in controlling HIV-1 and SIV replication, several vaccine strategies are being pursued for generating HIV-1-specific CTLs (5, 7, 9, 15, 22, 23). Currently, the most promising vaccine strategy for the induction of CTL responses seems to be a heterologous prime/boost regimen employing a plasmid DNA prime dose and a live recombinant-vector boost dose. Since the immunogenicity of plasmid DNA has proved to be modest in human clinical trials, our attempt is to construct a protein-based vaccine capable of inducing potent HIV-1-specific cellular immunity.

Nanoparticles (NPs) are considered to be an efficient antigen carrier and have been widely investigated for their biological potential (20, 21). NPs of an appropriate size are efficiently taken up by dendritic cells (DCs) and can present the carried antigens along with major histocompatibility complex (MHC) class I molecules to CD8$^+$ T cells through the antigen cross-presentation pathway (6, 8, 16). DCs are professional antigen-presenting cells capable of stimulating naïve T cells in the primary immune response and are more-potent antigen-presenting cells than monocyte/macrophages or B cells (4). The superiority of DCs in immunostimulatory activity involves the high-level expression of MHC and costimulatory molecules (CD40, CD80, and CD86), as well as the ability to produce T-helper 1 (Th1) cytokines, such as interleukin-12 (IL-12) and alpha interferon (IFN-α) (4). The ability of DCs to prime naïve T cells with antigens and their presence in various peripheral tissues imply a central role of DCs in mediating immune responses to infectious diseases and cancers.

We have previously reported that antigen-carrying core-corona polystyrene NPs (PSNPs) were efficiently taken up by DCs and did enhance the immunogenicity of antigens (28, 29). Intranasal immunization of mice with heat-inactivated HIV-1-capturing PSNPs demonstrated efficient production of HIV-1-specific neutralizing antibodies in the genital tract and CTL responses in the spleen (2, 10). Furthermore, intranasal immunization with inactivated simian-human immunodeficiency virus (SHIV)-capturing NPs (SHIV-NPs) could induce mucosal immune responses in macaques, and the macaques immunized with SHIV-NPs were partially protected from vaginal and systemic challenge with SHIV (18). However, nonbiodegradable PSNPs may not be applicable in clinical situations as a vaccine

* Corresponding author. Mailing address: Division of Antiviral Chemotherapy, Center for Chronic Viral Diseases, Graduate School of Medical and Dental Sciences, Kagoshima University, 8-35-1, Sakuragaoka, Kagoshima 890-8544, Japan. Phone: 81 99-275-5930. Fax: 81 99-275-5932. E-mail: m-baba@vanilla.ocn.ne.jp.

$^\nabla$ Published ahead of print on 3 July 2007.

material because of their safety issues. To circumvent this problem, we have recently created a novel biodegradable antigen delivery system with self-assembled polymeric NPs using poly(γ-glutamic acid) (γ-PGA) (1). NPs composed of amphiphilic γ-PGA and hydrophobic amino acids can immobilize proteins, peptides, and chemicals onto their surfaces and/or encapsulate these substances into the particles. In addition, γ-PGA NPs were found to be an efficient protein antigen delivery system and adjuvant to DCs in vitro and in vivo (26).

MATERIALS AND METHODS

Preparation of γ-PGA NPs. γ-PGA (number-average molecular weight, M_n, 380,000) was kindly provided by Meiji Seika Co., Ltd., Tokyo, Japan. The synthesis procedures for γ-PGA NPs, PSNPs, and protein-carrying γ-PGA NPs have been described in our previous report (1, 10). Recombinant HIV-1 (III_B strain) gp120 protein (Immuno Diagnostics, Woburn, MA) was chosen for the immunization experiments and either immobilized onto or encapsulated into γ-PGA NPs. To prepare the gp120-immobilizing γ-PGA NPs [gp120-NPs (imz)], the carboxyl group of the γ-PGA NPs (10 mg/ml) was activated by water-soluble carbodiimide for 20 min. The NPs, obtained by centrifugation (14,000 × *g* for 15 min), were mixed with 1 ml of gp120 (0.5 mg/ml) in phosphate-buffered saline (PBS), and the mixture was incubated at 4°C for 24 h. After the reaction, the centrifuged NPs were washed twice with PBS. The gp120-immobilizing PSNPs [gp120-PSNPs (imz)] were prepared by the same method. To prepare the gp120-encapsulating γ-PGA NPs [gp120-NPs (ecp)], γ-PGA-graft-L-phenylalanine ethylester (10 mg/ml) in dimethyl sulfoxide was added to the same volume of gp120 (0.75 mg/ml) in PBS. After the reaction, the centrifuged NPs were washed twice with PBS. The amount of entrapped gp120 protein was evaluated by the Lowry method, as previously described (1). The particle sizes of γ-PGA NPs and protein-carrying γ-PGA NPs in aqueous solution were measured by a dynamic light scattering method. The mean diameters of γ-PGA NPs, PSNPs, gp120-NPs (imz), gp120-NPs (ecp), and gp120-PSNPs (imz) were 210 ± 67 (mean ± standard deviation), 267 ± 76, 301 ± 127, 450 ± 124, and 316 ± 93 nm, respectively. The NPs did not form larger aggregates after they had been mixed with or conjugated to HIV-1 antigens. To determine the distribution of the antigen carried by γ-PGA NPs, fluorescein 5-isothiocyanate-conjugated ovalbumin (FITC-OVA) (Molecular Probes, Inc., Eugene, OR) was selected as a model antigen. FITC-OVA was encapsulated into γ-PGA NPs with the method described above.

Mice and immunization. Six- to 8-week-old female BALB/c mice were purchased from Charles River Japan (Yokohama, Japan). The experiments were carried out in accordance with the guidelines for animal experimentation in Kagoshima University. The mice were anesthetized by an intraperitoneal injection of sodium pentobarbital and intranasally immunized with various concentrations of antigens in a total volume of 20 μl to one nostril.

Proliferation assay. Spleen lymphocytes from the immunized mice were isolated by lympholyte-M (Cedarlane, Ontario, Canada) and tested in a standard [^{3}H]thymidine incorporation assay. The cells were cultured in a 96-well flat-bottom plate (2 × 10^5/well) with gp120 protein or the p18 epitope peptide (RGPGRAFVTI) (25) at various concentrations. They were incubated for 5 days at 37°C and pulsed with 1 μCi of [^{3}H]thymidine per well for 16 h. The cells were harvested on a glass filter paper, and their radioactivity was measured with a liquid scintillation counter. The mean count per min from triplicate wells was used for calculating the stimulation index. The stimulation index is the count per min with antigen stimulation divided by the count per min with stimulation with medium alone.

Pentamer staining and flow cytometric analysis. Pentameric H-2D^d complexes folded with the p18 epitope peptide (25) were purchased from Proimmune (Oxford, United Kingdom). Spleen lymphocytes from the immunized mice were stained with the p18 pentamer conjugated with allophycocyanin and an FITC-conjugated anti-CD8α monoclonal antibody (MAb) (KT-15; Proimmune) to detect p18-specific CD8$^+$ T cells. The cells were washed in PBS containing 0.1% sodium azide and 0.1% bovine serum albumin and fixed with PBS containing 2.5% formaldehyde (Wako, Tokyo, Japan). For phenotyping of the p18-specific CD8$^+$ T cells, spleen lymphocytes were collected at certain time points after immunization and stained with a peridinin chlorophyll protein-Cy5.5-conjugated anti-CD8α MAb (53-6.7; BD Biosciences, San Jose, CA), a phycoerythrin (PE)-conjugated anti-CD44 MAb (IM7; eBioscience, San Diego, CA), an FITC-conjugated anti-CD62L MAb (MEL-14; eBioscience), a PE-conjugated anti-CD127 MAb (A7R34; eBioscience), and the allophycocyanin-conjugated p18 pentamer. The cells were washed with PBS, and the levels of cell-associated fluorescence were determined by using a multicolor flow cytometer (FACSCalibur; BD Biosciences) and analyzed with CellQuest software (BD Biosciences).

IFN-γ ELISPOT assay. An enzyme-linked immunospot (ELISPOT) assay was performed to measure IFN-γ production. Spleen lymphocytes from the immunized mice were cultured in a plate with medium alone, the p18 epitope peptide (5 μg/ml), or gp120 protein (5 μg/ml). After a 24-h incubation at 37°C, the plate was washed, and the IFN-γ-producing cells were measured with an ELISPOT assay kit (BD Biosciences), according to the manufacturer's instructions. The data were expressed as the mean number of spot-forming units per million cells ± the standard error of the mean (SEM).

Intracellular cytokine staining and flow cytometric analysis. Spleen lymphocytes from the immunized mice were stimulated with the p18 epitope peptide (10 μg/ml) or medium alone for 6 h. The protein transport inhibitor BD GolgiPlug (1:1,000; BD Biosciences) was added to accumulate intracellular cytokines. The cells were washed, incubated for 10 min at 4°C with a purified anti-mouse CD16/32 to block Fc receptors, and stained with a PE-conjugated anti-CD8α MAb (53-6.7; BD Biosciences) for 30 min at 4°C. The cells were permeabilized (BD Cytofix/Cytoperm Plus; BD Biosciences) and stained with an FITC-conjugated anti-IFN-γ MAb (XMG 1.2; BD Biosciences), an FITC-conjugated anti-IL-2 MAb (JES6-5H4; BD Biosciences), or an FITC-conjugated anti-tumor necrosis factor alpha (TNF-α) MAb (MP6-XT22; BD Biosciences) for 30 min at 4°C. The cells were washed with PBS, and the levels of cell-associated fluorescence were determined by using a FACSCalibur and analyzing with CellQuest.

CTL assay. Spleen lymphocytes from the immunized mice were suspended in RPMI 1640 medium supplemented with 10% heat-inactivated fetal bovine serum, 100 U/ml penicillin, 100 μg/ml streptomycin, 50 mM 2-mercaptoethanol, and 20 U/ml recombinant IL-2 (Sigma, St. Louis, MO). The cells (4 × 10^6 cells/ml) were cultured with the p18 epitope peptide (10 μg/ml) in a 24-well plate for 4 days. MHC-matched P815 cells (H-2^d) were used as the target cells. The target cells (1 × 10^5 cells/ml) were preincubated with the p18 epitope peptide (10 μg/ml) for 16 h. The cytolytic activity of the effector cells was evaluated with a lactate dehydrogenase (LDH) cytotoxicity detection assay kit (Takara, Tokyo, Japan), as previously described (11). Prior to the assay, dead cells were removed from the effector cells by density gradient centrifugation with lympholyte-M. The effector and peptide-pulsed target cells were cocultured in a 96-well round-bottom plate at various effector/target ratios. After being incubated for 4 h, the culture supernatants were harvested and examined for their LDH levels. The LDH level of cell-free medium (background) was subtracted from the LDH levels of the samples. The percent specific lysis was calculated as follows: (sample LDH − effector spontaneous LDH − target spontaneous LDH)/(target maximum LDH − target spontaneous LDH) × 100. The effector and target spontaneous LDH levels were determined by culturing the cells with medium alone, and the target maximum LDH level was determined by adding 1% Triton X-100 to the target cells. To clarify the roles of CD4$^+$ and CD8$^+$ T cells in gp120-NP-induced cytolytic activity, an anti-CD4 MAb (GK1.5; eBioscience) and an anti-CD8 MAb (53-6.7; eBioscience) were used for depletion of CD4$^+$ and CD8$^+$ T cells, respectively. The MAbs were mixed with the effector cells before being added to the target cells at a final concentration of 10 μg/ml and incubated for 45 min at 4°C.

Statistical analysis. Statistical tests were performed by using Student's *t* test. A *P* value of less than 0.05 was considered significant.

RESULTS

Induction of antigen-specific CD8$^+$ T cells by gp120-NPs. Since γ-PGA NPs act as an efficient protein antigen delivery system and adjuvant to DCs in vitro and in vivo (26), the ability of γ-PGA NPs to elicit HIV-1-specific CD8$^+$ T-cell responses was examined in mice. Recombinant HIV-1 gp120 protein was selected as an immunogen, and gp120-NPs (ecp) and gp120-NPs (imz) were created. The mice were intranasally immunized once with gp120-NPs, and their cellular immune responses were measured with a lymphocyte proliferation assay. As shown in Fig. 1, antigen-specific lymphocyte proliferation was not observed in the spleen lymphocytes obtained from the mice immunized with PBS, gp120 alone, or NPs alone. In contrast, the spleen cells obtained from the mice immunized with gp120-NPs (ecp) and gp120-

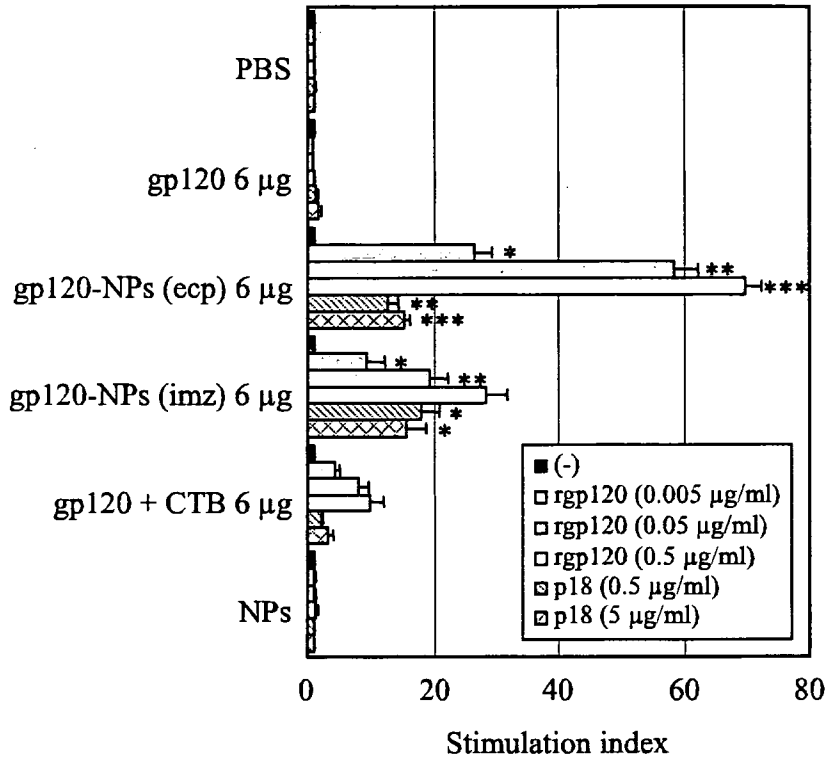

FIG. 1. Induction of antigen-specific lymphocyte proliferation by gp120-NPs. Mice were intranasally immunized once with the indicated antigens. Spleen lymphocytes were isolated on day 10 after immunization and stimulated in vitro with the indicated concentrations of the recombinant gp120 (rgp120) or p18 peptide for 5 days. The cells were exposed to [^{3}H]thymidine for the final 16 h, and the levels of incorporation of radioactivity were determined. All data represent the means ± SEMs of the results for four mice per group. Statistical analysis was carried out in comparison with the results for the gp120 + CTB group. −, no stimulus; *, $P < 0.05$; **, $P < 0.01$; ***, $P < 0.001$.

NPs (imz) showed significant antigen-specific proliferation in a dose-dependent fashion compared to the proliferation in the spleen cells obtained from mice immunized with a mixture of gp120 and the B-subunit of cholera toxin (gp120 + CTB) (Fig. 1). Higher lymphocyte proliferation was observed in the mice immunized with gp120-NPs (ecp) than in those immunized with gp120-NPs (imz). Furthermore, both gp120-NPs (ecp) and gp120-NPs (imz) elicited potent p18-specific lymphocyte proliferation. These results suggest that both gp120-NPs (ecp) and gp120-NPs (imz) have great potential to induce antigen-specific cellular immune responses, especially, $CD8^+$ T-cells.

When the $CD8^+$ T-cell responses to the H-2^d-restricted p18 epitope were examined with the pentamer-staining assay, immunization with gp120-NPs (ecp) and gp120-NPs (imz) had strongly induced p18-specific $CD8^+$ T-cell responses in a dose-dependent fashion (Fig. 2A). Higher responses were observed even in the mice immunized with gp120-NPs at a dose of 0.24 μg than in those immunized with gp120 alone or gp120 + CTB at a dose of 6 μg. Although the immune responses induced by gp120-NPs (ecp) and gp120-NPs (imz) were comparable at a dose of 6 μg, stronger $CD8^+$ T-cell responses were induced by gp120-NPs (ecp) than by gp120-NPs (imz) at a dose of 1.2 μg. Surprisingly, a simple mixture of gp120 and NPs (gp120 + NPs) could also induce potent p18-specific $CD8^+$ T-cell responses in mice (Fig. 2A).

The functional capacity of gp120-NP-induced specific $CD8^+$ T cells was assessed with an IFN-γ ELISPOT assay following stimulation with the p18 peptide and gp120. As shown in Fig. 2B, a number of p18- and gp120-specific IFN-γ-producing cells were identified in the mice immunized with gp120-NPs, and the IFN-γ-producing cells were more abundant than those in the mice receiving gp120 + CTB (Fig. 2B). No antigen-specific IFN-γ-producing cells were detected in the mice immunized with PBS or gp120 alone. Similar to the results of pentamer staining (Fig. 2A), gp120-NPs (ecp) were a more potent inducer of the IFN-γ-producing cells than gp120-NPs (imz) at a dose of 1.2 μg of gp120. Again, gp120 + NPs also potently induced the IFN-γ-producing cells in mice. When the production of IL-2 and TNF-α from the antigen-specific $CD8^+$ T cells was evaluated by intracellular cytokine staining, both cytokines could be detected for the cells obtained from the gp120-NP-immunized mice (Fig. 2C). Similar to the ELISPOT results, the production of these cytokines was also higher in the mice immunized with gp120-NPs (ecp) than in those immunized with gp120-NPs (imz).

To assess the cytolytic activities of gp120-NP-induced $CD8^+$ T cells, spleen lymphocytes from the immunized mice were cultured with the p18 peptide for 4 days and used as the effector cells. As shown in Fig. 2D, p18-specific cytotoxic activity was not observed for the spleen lymphocytes of the mice immunized with gp120 alone or gp120 + CTB. In contrast, the spleen lymphocytes of the mice immunized with gp120-NPs (ecp) or gp120-NPs (imz) displayed significant cytolytic activity

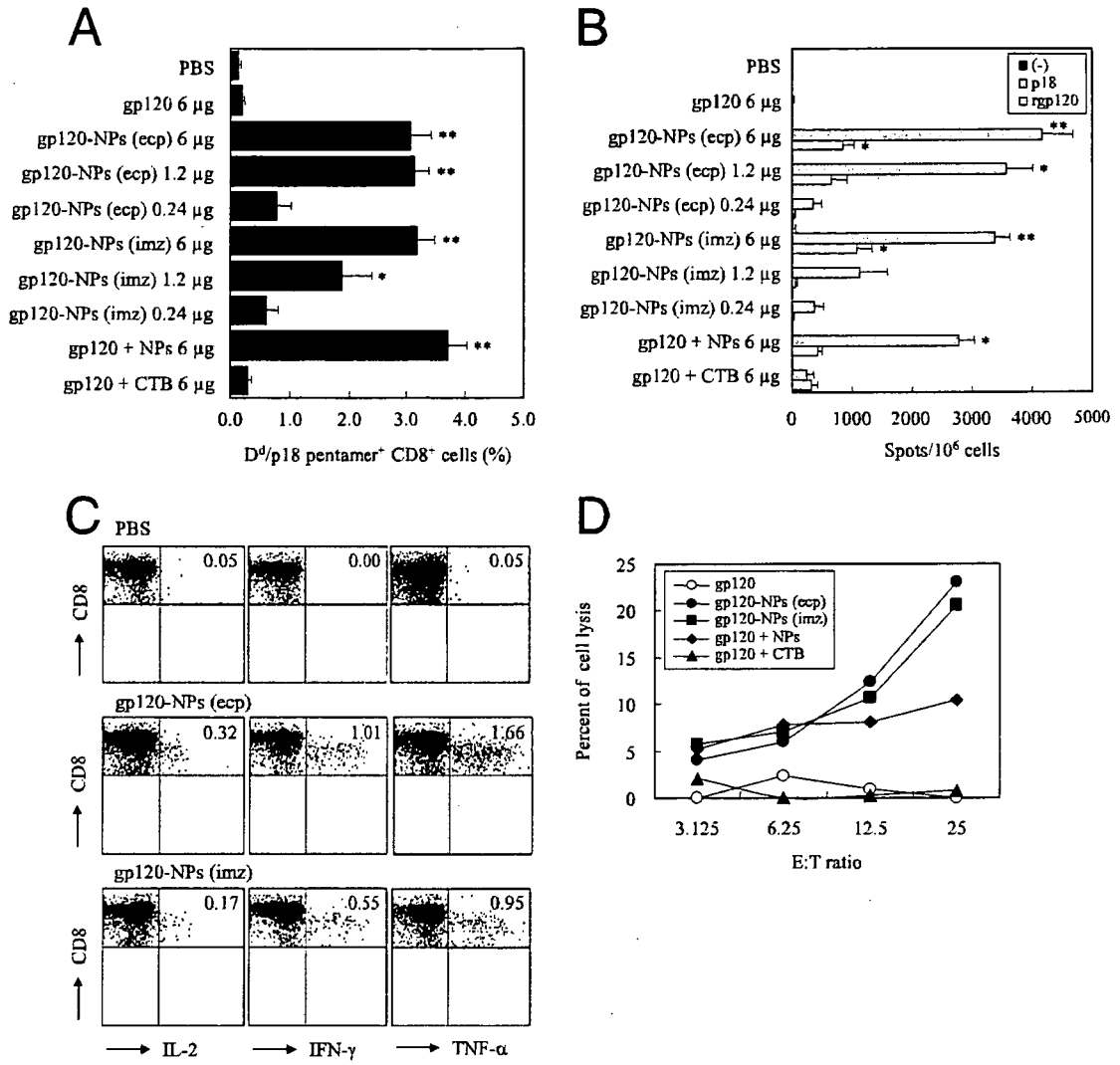

FIG. 2. Induction of gp120-specific CD8$^+$ T-cell responses by gp120-NPs. Mice were intranasally immunized once with the indicated antigens. Spleen lymphocytes were isolated on day 10 after immunization. (A) Antigen-specific CD8$^+$ T cells were detected by H-2D^d/p18 pentamer staining. Data are expressed as the percentages of the gated CD8$^+$ T cells that bound to the pentamer, as measured by flow cytometry. All data represent the mean ± SEM of the results for four mice per group. Statistical analysis was carried out in comparison with the results for the gp120 + CTB group. *; $P < 0.05$; **; $P < 0.001$. (B) Spleen lymphocytes were evaluated by ELISPOT for IFN-γ production after stimulation with no peptide (−), the p18 peptide (5 μg/ml), or recombinant gp120 (rgp120; 5 μg/ml). Data are expressed as the numbers of antigen-specific spots per million cells. All data represent the mean ± SEM of the results for four mice per group. Statistical analysis was carried out in comparison with the results for the gp120 + CTB group. *, $P < 0.05$; **, $P < 0.001$. (C) CD8$^+$ T cells were evaluated by intracellular cytokine staining for the production of IL-2, IFN-γ, and TNF-α after stimulation with the p18 peptide. Data are expressed as the percentages of cytokine-positive CD8$^+$ cells. (D) Spleen lymphocytes were cultured for 4 days in the presence of the p18 peptide (10 μg/ml). The cells were harvested and used as effector cells to assess P815 target cell lysis by measuring LDH release after overnight incubation with medium alone or the p18 peptide. Data are expressed as the levels of peptide-specific lysis, calculated by subtracting the percent specific lysis of the control target cells from the percent specific lysis of the peptide-pulsed target cells at the indicated effector-to-target (E:T) cell ratio.

for the target cells. Modest cytolytic activity was observed for the spleen lymphocytes of the mice immunized with gp120 + NPs. These results indicate that the antigen-specific CD8$^+$ T cells induced by gp120-NPs are capable of secreting IFN-γ, IL-2, and TNF-α and functioning as CTLs.

Comparison of γ-PGA NPs with PSNPs for the induction of antigen-specific CD8$^+$ T cells. To compare the efficacy of γ-PGA NPs and PSNPs in inducing antigen-specific CD8$^+$ T-cell responses, the binding of H-2D^d/p18 pentamers to CD8$^+$ T cells was evaluated on day 10 after immunization with gp120-NPs (imz) or gp120-PSNPs (imz). As shown in Fig. 3A, gp120-NPs (imz) could induce the p18-specific CD8$^+$ T-cell responses more strongly than gp120-PSNPs (imz) and gp120 alone. Furthermore, the p18-specific IFN-γ-producing cells were identified as being more abundant in the mice immunized with gp120-NPs (imz) than in the mice receiving gp120-PSNPs (imz) (Fig. 3B). These results indicate that γ-PGA NPs are superior to PSNPs as an inducer of antigen-specific CD8$^+$ T cells.

Induction of long-lived memory CD8$^+$ T cells. To determine whether intranasal immunization with gp120-NPs could gen-

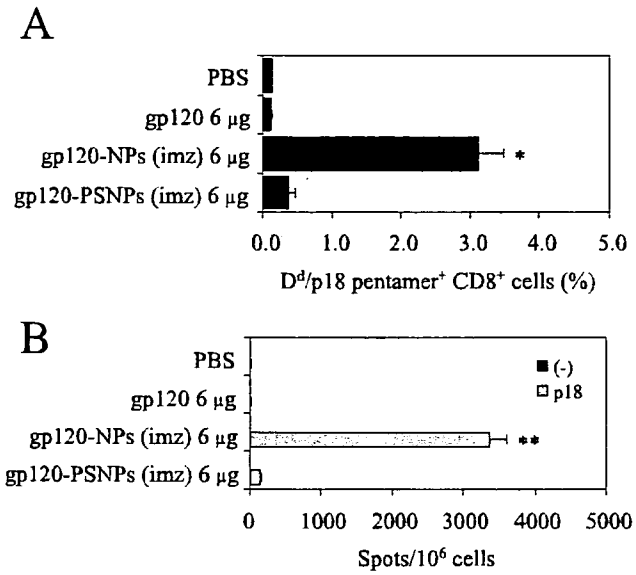

FIG. 3. Induction of gp120-specific $CD8^+$ T-cell responses by gp120-NPs (imz) and gp120-PSNPs (imz). Mice were intranasally immunized once with the indicated antigens. Spleen lymphocytes were isolated on day 10 after immunization. (A) Antigen-specific $CD8^+$ T cells were detected by H-$2D^d$/p18 pentamer staining. Data are expressed as the percentages of the gated $CD8^+$ T cells that bound to the pentamer, as measured by flow cytometry. All data represent the means ± SEMs of the results for three mice per group. Statistical analysis was carried out in comparison with the results for the gp120-PSNPs group. *, $P < 0.05$. (B) Spleen lymphocytes were evaluated by ELISPOT for their IFN-γ production after stimulation with no peptide (−) or the p18 peptide (5 μg/ml). Data are expressed as the numbers of antigen-specific spots per million cells. All data represent the means ± SEMs of the results for three mice per group. Statistical analysis was carried out in comparison with the results for the gp120-PSNPs group. **, $P < 0.001$.

erate memory $CD8^+$ T cells, the spleen lymphocytes were harvested after 4 weeks of immunization and subjected to the IFN-γ ELISPOT and CTL assays. As shown in Fig. 4, considerable numbers of p18- and gp120-specific IFN-γ-producing cells were identified in the mice immunized with gp120-NPs.

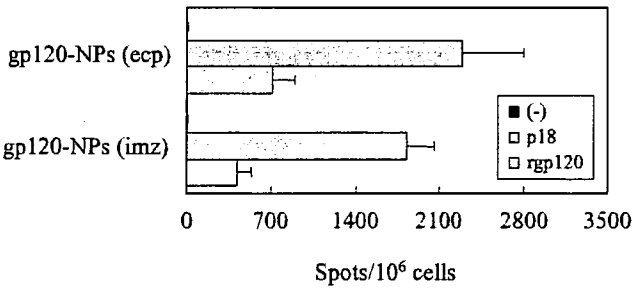

FIG. 4. Functional analysis of the memory $CD8^+$ T cells. Mice were intranasally immunized once with 6 μg of gp120-NPs. Spleen lymphocytes were collected on day 30 after immunization. Spleen lymphocytes were evaluated by ELISPOT for their IFN-γ production after stimulation with no peptide (−), the p18 peptide (5 μg/ml), or recombinant gp120 (rgp120; 5 μg/ml). Data are expressed as the numbers of antigen-specific spots per million cells. All data represent the means ± SEMs of the results for four mice per group.

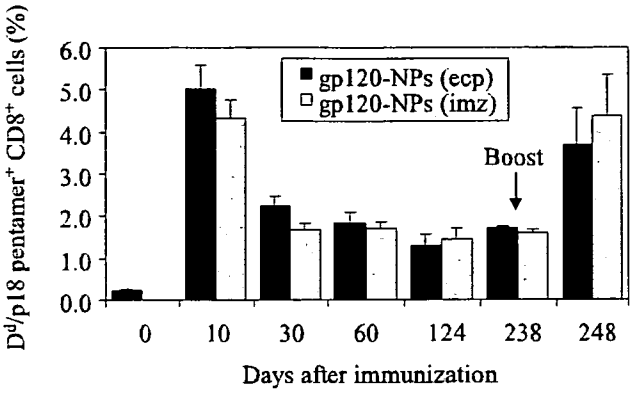

FIG. 5. Long-lived p18-specific memory $CD8^+$ T cells induced by gp120-NPs. Mice were intranasally immunized once with 6 μg of gp120-NPs. On day 238, mice were boosted with the same gp120-NPs as those used for the first immunization. Spleen lymphocytes were collected from the immunized mice at the indicated times, and antigen-specific $CD8^+$ T cells were detected by H-$2D^d$/p18 pentamer staining. Data are expressed as the percentages of the gated $CD8^+$ T cells that bound to the pentamer, as measured by flow cytometry. All data represent the means ± SEMs or range of the results for two to four mice per group.

Again, gp120-NPs (ecp) were a more potent inducer of the IFN-γ-producing cells than gp120-NPs (imz). Furthermore, the cells could efficiently kill the target cells pulsed with the p18 peptide (data not shown). These results suggest that a pool of the antigen-specific memory $CD8^+$ T cells was generated after 4 weeks.

To determine whether the antigen-specific memory $CD8^+$ T cells were long-lived or not, the binding of the H-$2D^d$/p18 pentamer to $CD8^+$ T cells was evaluated at the indicated times after the immunization with gp120-NPs. As shown in Fig. 5, both gp120-NPs (ecp) and gp120-NPs (imz) displayed similar kinetics of p18-specific $CD8^+$ T-cell responses. After a peak in the number of pentamer-positive cells on day 10, the positive cell number decreased on day 30 and remained stable from day 30 to day 238. However, the pentamer-positive cell number rapidly increased again immediately after boosting with gp120-NPs. To further characterize the antigen-specific memory $CD8^+$ T cells, their maturation stages were determined by assessing the surface expression of CD44, CD127, and CD62L on day 30 after immunization by using flow cytometry. All of the pentamer-positive cells expressed CD44, indicating that they were activated (Fig. 6A). Most of the cells had the profiles of effector memory cells (pentamer positive, $CD127^+$, and $CD62L^{low}$), and substantial decay of these cells was observed over time (Fig. 6A and 6B). On the other hand, the number of central memory cells (pentamer positive, $CD127^+$, and $CD62L^{high}$) was lower than the number of effector memory cells. The number of central memory cells remained relatively constant and tended to increase between days 30 and 238 after immunization. There was no significant difference between gp120-NP (ecp) and gp120-NP (imz) immunization in the resulting levels and subsets of memory cells. These results indicate that gp120-NPs can generate both effector and long-lived central memory HIV-1-specific $CD8^+$ T cells.

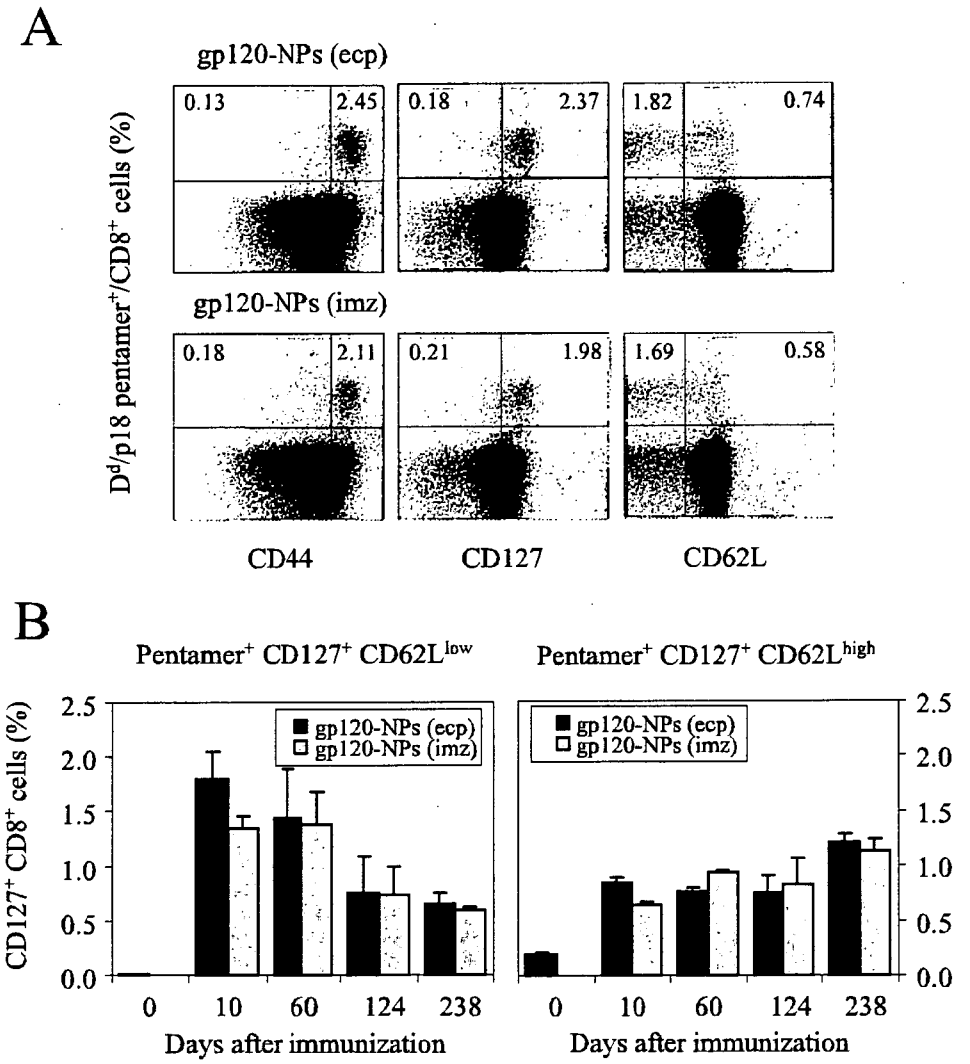

FIG. 6. Analysis of antigen-specific CD8$^+$ central and effector memory T cells induced by gp120-NPs. Mice were intranasally immunized once with 6 μg of gp120-NPs. (A) Spleen lymphocytes were collected from the immunized mice on day 30 and examined by flow cytometry for the expression of CD44, CD127, and CD62L in the H-2D^d/p18 pentamer-positive CD8$^+$ T cells. The numbers in the upper left and right corners of each panel indicate the percentages of H-2D^d/p18 pentamer-positive and indicated marker (CD44, CD127, or CD62L) low and high CD8$^+$ T cells, respectively. (B) Spleen lymphocytes were collected from the immunized mice at the indicated times and examined for the expression of CD127 and CD62L on the H-2D^d/p18 pentamer-positive CD8$^+$ T cells by flow cytometry. Data are expressed as the percentages of CD127$^+$ CD8$^+$ T cells. All data represent the means ± SEMs or range of the results for two to four mice per group.

DISCUSSION

The results presented here demonstrate that novel biodegradable γ-PGA NPs hold great promise as an antigen delivery system and effective adjuvant for inducing HIV-1-specific cellular immune responses. Protein-based vaccines generally induce strong MHC class II-mediated humoral immune responses but weak MHC class I-mediated cellular immune responses. It was reported that the encapsulation of protein antigens into NPs could modulate certain immune responses, including the enhancement of CTL against the particle-associated antigen (17, 19). DCs are considered to be an initiator and modulator of immune responses and capable of presenting antigens through both MHC class I and II pathways. The cells efficiently take up poly(D,L-lactate-co-glycolide) NPs of an appropriate size and present particle-associated antigens along with MHC class I molecules to CD8$^+$ T cells through the antigen cross-presentation pathway (6, 8, 16). γ-PGA NPs were found to deliver protein antigens to DCs in vitro and in vivo (26). Furthermore, our preliminary data suggest that γ-PGA NPs could also efficiently deliver the encapsulated antigen into CD11c$^+$ and CD86$^+$ cells with low granularity in the lung, which were considered to be pulmonary DCs, after intranasal administration (data not shown). Thus, targeting of protein antigen to DCs appears to be an important mechanism of γ-PGA NPs in inducing HIV-1-specific cellular immune responses.

Cellular immunity plays a critical role in controlling HIV-1 replication in the acute phase of infection and maintaining a

low viral load in the chronic phase. Therefore, an effective anti-AIDS vaccine should induce potent CTLs against HIV-1 antigen-expressing cells. In fact, the $CD8^+$ T cells induced by gp120-NPs exhibited effector functions, such as cytolytic activity and the production of various cytokines (Fig. 2). Such $CD8^+$ T cells seem to play a critical role in protecting against disease progression in SIV-infected monkeys (13, 24). In comparison with gp120-NPs (imz), gp120-NPs (ecp) showed a slightly better ability to induce functional antigen-specific $CD8^+$ T cells (Fig. 2B, 2C, and 2D). To our surprise, either gp120-NPs (ecp) or gp120-NPs (imz) induced low, if any, levels of gp120-specific antibodies in sera and vaginal fluids of the mice even after four intranasal immunizations (data not shown), whereas the mice immunized with gp120 + CTB had high levels of gp120-specific antibodies in both sera and vaginal fluids. Thus, γ-PGA NPs are different from CTB and have the ability to potently induce cellular immunity rather than humoral immunity through intranasal immunization. Since an efficacious vaccine against HIV-1 should elicit both humoral and cellular responses, the modification of γ-PGA NPs for eliciting both humoral and cellular responses, especially for the production of immunoglobulin A antibodies on the mucous membrane, is now under investigation. Another interesting observation is that even gp120 + NPs could induce considerable cellular immunity (Fig. 2A, 2B, and 2D), probably because negatively charged γ-PGA NPs adsorbed positively charged gp120 on their surface and thereby behaved like gp120-NPs (imz). These results suggest that, although it may not be applicable to all antigens, a simple mixture of some antigens and γ-PGA NPs is more practical as a vaccine formulation in developing protein-based vaccines than antigen-encapsulating or -immobilizing γ-PGA NPs.

An ideal priming vector for inducing cellular immune responses should elicit a large population of $CD8^+$ T cells that differentiate rapidly into memory cells, which will generate vigorous secondary immune responses immediately after boosting. In our study, the antigen-specific $CD8^+$ T cells induced by gp120-NPs rapidly differentiated to the memory cells on day 30 and retained a stable level from day 30 to day 238 (Fig. 5). These memory $CD8^+$ T cells rapidly exhibited effector functions, such as antigen-specific cytotoxicity and IFN-γ production after in vitro stimulation (Fig. 4 and data not shown). Furthermore, the memory $CD8^+$ T cells rapidly expanded in vivo after being boosted with the same antigen (Fig. 5). The characterization of the memory $CD8^+$ T cells revealed that the majority of the cells were effector memory cells on day 30, yet central memory cells also existed and stayed stable for more than 200 days after immunization (Fig. 6). It is noteworthy that intranasal immunization of mice only once with gp120-NPs could induce a stable population of antigen-specific central memory $CD8^+$ T cells. The ability of gp120-NPs to generate the long-lived central memory cells is particularly important, since these cells expand and mediate protective immunity after a challenge with pathogens (24, 30). Further studies are needed to determine whether antigen-carrying γ-PGA NPs have such activity in other species.

The factors that regulate the differentiation of $CD8^+$ T cells to memory cells have not been fully understood yet. Several events, such as inflammation, DC maturation, and antigen persistence, affect the differentiation process. It was recently shown that the vaccination of mice with peptide-pulsed mature DCs resulted in accelerated differentiation of memory $CD8^+$ T cells (3). Indeed, γ-PGA NPs upregulated the expression of MHC and costimulatory molecules of DCs in vitro and in vivo (26). Furthermore, γ-PGA NPs could also induce the production of inflammatory cytokines from DCs. These finding indicate that γ-PGA NPs are capable of inducing the maturation of DCs, which may rapidly generate memory $CD8^+$ T cells.

In conclusion, the present work demonstrates the ability of gp120-carrying γ-PGA NPs to induce robust cellular immune responses in mice. Thus, γ-PGA NPs may have great potential as an antigen carrier and novel protein-based vaccine against HIV-1 infection.

ACKNOWLEDGMENT

This work was supported by Core Research for Evolutional Science and Technology (CREST) from the Japan Science and Technology Agency (JST).

REFERENCES

1. **Akagi, T., T. Kaneko, T. Kida, and M. Akashi.** 2005. Preparation and characterization of biodegradable nanoparticles based on poly(γ-glutamic acid) with L-phenylalanine as a protein carrier. J. Control. Release **108**:226–236.
2. **Akagi, T., M. Kawamura, M. Ueno, K. Hiraishi, M. Adachi, T. Serizawa, M. Akashi, and M. Baba.** 2003. Mucosal immunization with inactivated HIV-1-capturing nanospheres induces a significant HIV-1-specific vaginal antibody response in mice. J. Med. Virol. **69**:163–172.
3. **Badovinac, V. P., K. A. Messingham, A. Jabbari, J. S. Haring, and J. T. Harty.** 2005. Accelerated $CD8^+$ T-cell memory and prime-boost response after dendritic-cell vaccination. Nat. Med. **11**:748–756.
4. **Banchereau, J., F. Briere, C. Caux, J. Davoust, S. Lebecque, Y. J. Liu, B. Pulendran, and K. Palucka.** 2000. Immunobiology of dendritic cells. Annu. Rev. Immunol. **18**:767–811.
5. **Borrow, P., H. Lewicki, X. Wei, M. S. Horwitz, N. Peffer, H. Meyers, J. A. Nelson, J. E. Gairin, B. H. Hahn, M. B. Oldstone, and G. M. Shaw.** 1997. Antiviral pressure exerted by HIV-1-specific cytotoxic T lymphocytes (CTLs) during primary infection demonstrated by rapid selection of CTL escape virus. Nat. Med. **3**:205–211.
6. **Fonteneau, J. F., D. G. Kavanagh, M. Lirvall, C. Sanders, T. L. Cover, N. Bhardwaj, and M. Larsson.** 2003. Characterization of the MHC class I cross-presentation pathway for cell-associated antigens by human dendritic cells. Blood **102**:4448–4455.
7. **Goonetilleke, N., S. Moore, L. Dally, N. Winstone, I. Cebere, A. Mahmoud, S. Pinheiro, G. Gillespie, D. Brown, V. Loach, J. Roberts, A. Guimaraes-Walker, P. Hayes, K. Loughran, C. Smith, J. De Bont, C. Verlinde, D. Vooijs, C. Schmidt, M. Boaz, J. Gilmour, P. Fast, L. Dorrell, T. Hanke, and A. J. McMichael.** 2006. Induction of multifunctional human immunodeficiency virus type 1 (HIV-1)-specific T cells capable of proliferation in healthy subjects by using a prime-boost regimen of DNA- and modified vaccinia virus Ankara-vectored vaccines expressing HIV-1 Gag coupled to $CD8^+$ T-cell epitopes. J. Virol. **80**:4717–4728.
8. **Guermonprez, P., L. Saveanu, M. Kleijmeer, J. Davoust, P. Van Endert, and S. Amigorena.** 2003. ER-phagosome fusion defines an MHC class I cross-presentation compartment in dendritic cells. Nature **425**:397–402.
9. **Jin, X., D. E. Bauer, S. E. Tuttleton, S. Lewin, A. Gettie, J. Blanchard, C. E. Irwin, J. T. Safrit, J. Mittler, L. Weinberger, L. G. Kostrikis, L. Zhang, A. S. Perelson, and D. D. Ho.** 1999. Dramatic rise in plasma viremia after $CD8^+$ T cell depletion in simian immunodeficiency virus-infected macaques. J. Exp. Med. **189**:991–998.
10. **Kawamura, M., T. Naito, M. Ueno, T. Akagi, K. Hiraishi, I. Takai, M. Makino, T. Serizawa, K. Sugimura, M. Akashi, and M. Baba.** 2002. Induction of mucosal IgA following intravaginal administration of inactivated HIV-1-capturing nanospheres in mice. J. Med. Virol. **66**:291–298.
11. **Kawamura, M., X. Wang, T. Uto, K. Sato, M. Ueno, T. Akagi, K. Hiraishi, T. Matsuyama, M. Akashi, and M. Baba.** 2005. Induction of dendritic cell-mediated immune responses against HIV-1 by antigen-capturing nanospheres in mice. J. Med. Virol. **76**:7–15.
12. **Klein, M.** 2003. Prospects and challenges for prophylactic and therapeutic HIV vaccines. Vaccine **21**:616–619.
13. **Letvin, N.** 2006. Virus-specific cellular immune correlates of survival in vaccinated monkeys after SIV challenge. Retrovirology **3**(Suppl. 1):S20.
14. **Letvin, N. L.** 2002. Strategies for an HIV vaccine. J. Clin. Investig. **110**:15–20.
15. **Letvin, N. L., Y. Huang, B. K. Chakrabarti, L. Xu, M. S. Seaman, K. Beaudry, B. Korioth-Schmitz, F. Yu, D. Rohne, K. L. Martin, A. Miura, W. P. Kong, Z. Y. Yang, R. S. Gelman, O. G. Golubeva, D. C. Montefiori, J. R.**

Mascola, and G. J. Nabel. 2004. Heterologous envelope immunogens contribute to AIDS vaccine protection in rhesus monkeys. J. Virol. **78**:7490–7497.

16. **Lutsiak, M. E., D. R. Robinson, C. Coester, G. S. Kwon, and J. Samuel.** 2002. Analysis of poly(D,L-lactic-co-glycolic acid) nanosphere uptake by human dendritic cells and macrophages in vitro. Pharm. Res. **19**:1480–1487.
17. **Maloy, K. J., A. M. Donachie, D. T. O'Hagan, and A. M. Mowat.** 1994. Induction of mucosal and systemic immune responses by immunization with ovalbumin entrapped in poly(lactide-co-glycolide) microparticles. Immunology **81**:661–667.
18. **Miyake, A., T. Akagi, Y. Enose, M. Ueno, M. Kawamura, R. Horiuchi, K. Hiraishi, M. Adachi, T. Serizawa, O. Narayan, M. Akashi, M. Baba, and M. Hayami.** 2004. Induction of HIV-specific antibody response and protection against vaginal SHIV transmission by intranasal immunization with inactivated SHIV-capturing nanospheres in macaques. J. Med. Virol. **73**:368–377.
19. **Moore, A., P. McGuirk, S. Adams, W. C. Jones, J. P. McGee, D. T. O'Hagan, and K. H. Mills.** 1995. Immunization with a soluble recombinant HIV protein entrapped in biodegradable microparticles induces HIV-specific $CD8^+$ cytotoxic T lymphocytes and $CD4^+$ Th1 cells. Vaccine **13**:1741–1749.
20. **Otten, G., M. Schaefer, C. Greer, M. Calderon-Cacia, D. Coit, J. Kazzaz, A. Medina-Selby, M. Selby, M. Singh, M. Ugozzoli, J. zur Megede, S. W. Barnett, D. O'Hagan, J. Donnelly, and J. Ulmer.** 2003. Induction of broad and potent anti-human immunodeficiency virus immune responses in rhesus macaques by priming with a DNA vaccine and boosting with protein-adsorbed polylactide coglycolide microparticles. J. Virol. **77**:6087–6092.
21. **Otten, G. R., M. Schaefer, B. Doe, H. Liu, I. Srivastava, J. Megede, J. Kazzaz, Y. Lian, M. Singh, M. Ugozzoli, D. Montefiori, M. Lewis, D. A. Driver, T. Dubensky, J. M. Polo, J. Donnelly, D. T. O'Hagan, S. Barnett, and J. B. Ulmer.** 2005. Enhanced potency of plasmid DNA microparticle human immunodeficiency virus vaccines in rhesus macaques by using a priming-boosting regimen with recombinant proteins. J. Virol. **79**:8189–8200.
22. **Schmitz, J. E., M. J. Kuroda, S. Santra, V. G. Sasseville, M. A. Simon, M. A. Lifton, P. Racz, K. Tenner-Racz, M. Dalesandro, B. J. Scallon, J. Ghrayeb, M. A. Forman, D. C. Montefiori, E. P. Rieber, N. L. Letvin, and K. A. Reimann.** 1999. Control of viremia in simian immunodeficiency virus infection by $CD8^+$ lymphocytes. Science **283**:857–860.
23. **Seaman, M. S., L. Xu, K. Beaudry, K. L. Martin, M. H. Beddall, A. Miura, A. Sambor, B. K. Chakrabarti, Y. Huang, R. Bailer, R. A. Koup, J. R. Mascola, G. J. Nabel, and N. L. Letvin.** 2005. Multiclade human immunodeficiency virus type 1 envelope immunogens elicit broad cellular and humoral immunity in rhesus monkeys. J. Virol. **79**:2956–2963.
24. **Sun, Y., J. E. Schmitz, A. P. Buzby, B. R. Barker, S. S. Rao, L. Xu, Z. Y. Yang, J. R. Mascola, G. J. Nabel, and N. L. Letvin.** 2006. Virus-specific cellular immune correlates of survival in vaccinated monkeys after simian immunodeficiency virus challenge. J. Virol. **80**:10950–10956.
25. **Takahashi, H., Y. Nakagawa, C. D. Pendleton, R. A. Houghten, K. Yokomuro, R. N. Germain, and J. A. Berzofsky.** 1992. Induction of broadly cross-reactive cytotoxic T cells recognizing an HIV-1 envelope determinant. Science **255**:333–336.
26. **Uto, T., X. Wang, K. Sato, M. Haraguchi, T. Akagi, M. Akashi, and M. Baba.** 2007. Targeting of antigen to dendritic cells with poly(γ-glutamic acid) nanoparticles induces antigen-specific humoral and cellular immunity. J. Immunol. **178**:2979–2986.
27. Reference deleted.
28. **Wang, X., T. Akagi, M. Akashi, and M. Baba.** 2007. Development of core-corona type polymeric nanoparticles as an anti-HIV-1 vaccine. Mini-Rev. Org. Chem. **4**:51–59.
29. **Wang, X., T. Uto, K. Sato, K. Ide, T. Akagi, M. Okamoto, T. Kaneko, M. Akashi, and M. Baba.** 2005. Potent activation of antigen-specific T cells by antigen-loaded nanospheres. Immunol. Lett. **98**:123–130.
30. **Wherry, E. J., V. Teichgraber, T. C. Becker, D. Masopust, S. M. Kaech, R. Antia, U. H. von Andrian, and R. Ahmed.** 2003. Lineage relationship and protective immunity of memory CD8 T cell subsets. Nat. Immunol. **4**:225–234.

JOURNAL OF VIROLOGY, Aug. 2007, p. 8722–8729 Vol. 81, No. 16
0022-538X/07/$08.00+0 doi:10.1128/JVI.00253-07

Clathrin-Dependent Entry of Severe Acute Respiratory Syndrome Coronavirus into Target Cells Expressing ACE2 with the Cytoplasmic Tail Deleted▽

Yuuki Inoue,[1] Nobuyuki Tanaka,[1,4]* Yoshinori Tanaka,[1] Shingo Inoue,[3] Kouichi Morita,[3] Min Zhuang,[2] Toshio Hattori,[2] and Kazuo Sugamura[1]

Department of Microbiology and Immunology[1] and Department of Infectious and Respiratory Diseases,[2] Internal Medicine, Tohoku University Graduate School of Medicine, Sendai 980-8575, Japan; Department of Virology, Institute of Tropical Medicine, Nagasaki University, Nagasaki 852-8523, Japan[3]; and Division of Immunology, Miyagi Cancer Center Research Institute, Natori 981-1293, Japan[4]

Received 6 February 2007/Accepted 7 March 2007

The penetration of various viruses into host cells is accomplished by hijacking the host endocytosis machinery. In the case of severe acute respiratory syndrome coronavirus (SARS-CoV) infection, viral entry is reported to require a low pH in intracytoplasmic vesicles; however, little is known about how SARS-CoV invades such compartments. Here we demonstrate that SARS-CoV mainly utilizes the clathrin-mediated endocytosis pathway for its entry to target cells by using infectious SARS-CoV, as well as a SARS-CoV pseudovirus packaged in the SARS-CoV envelope. The SARS-CoV entered caveolin-1-negative HepG2 cells, and the entry was significantly inhibited by treatment with chlorpromazine, an inhibitor for clathrin-dependent endocytosis, and by small interfering RNA-mediated gene silencing for the clathrin heavy chain. Furthermore, the SARS-CoV entered COS7 cells transfected with the mutant of ACE2 with the cytoplasmic tail deleted, SARS-CoV receptor, as well as the wild-type ACE2, and their entries were significantly inhibited by treatment with chlorpromazine. In addition, ACE2 translocated into EEA1-positive early endosomes immediately after the virus attachment to ACE2. These results suggest that when SARS-CoV binds ACE2 it is internalized and penetrates early endosomes in a clathrin-dependent manner and that the cytoplasmic tail of ACE2 is not required for the penetration of SARS-CoV.

Severe acute respiratory syndrome (SARS) is an emerging infectious disease with high mortality caused by infection of the respiratory system by SARS coronavirus (SARS-CoV). SARS-CoV is a human enveloped coronavirus containing a helical nucleocapsid structure composed of a single-stranded, positive-polarity RNA of approximately 29 kb plus the poly(A) tail (44). Phylogenetic analysis classifies the coronaviruses into three groups based on their genetic and serological relationships.

The first essential step in virus infection is the entry of viruses into host cells. After their attachment to their respective cell surface receptor, most viruses make use of cellular endocytosis machineries, such as clathrin-dependent and -independent pathways, for their entry (22, 29). Clathrin-dependent endocytosis has been well characterized using growth factor receptors such as the transferrin receptor (23), epidermal growth factor receptor (EGFR) (39), and the keratinocyte growth factor receptor (3). The endocytosed receptors are translocated into endosomes, where they are degraded or recycled to the cell surface. Similarly, various viruses, among them Semliki Forest virus, vesicular stomatitis virus (VSV), and influenza virus, enter into host cells via the clathrin-dependent endocytosis pathway and translocate into endosomes, where they are uncoated (10, 35, 40). The clathrin-dependent endocytosis is initiated by the binding of adaptor protein 2 (AP2) complexes to the cytoplasmic tail of the cell-surface receptors, which recruits clathrins (27, 38). Subsequently, the receptors are invaginated to form "pits," which are surrounded by a spherical cage-like structure made of clathrin triskelions. Viruses bound to the receptors are endocytosed similarly and then transported to vesicles called early endosomes. It is well known that early endosomes are somewhat acidic (pH 6.5 to 6.0) and become more acidic as they mature to form late endosomes (pH 6.0 to 5.5). The acidification of endosomes is required for incorporated viruses to establish an infection (22, 29).

On the other hand, the clathrin-independent pathways include a caveola-dependent pathway. Caveolae are relatively smaller vesicles of 50 to 100 nm in diameter, formed by membrane invagination at the cell surface, and coated by caveolin-1 (12, 15, 28). Simian virus 40 (SV40), for example, utilizes caveolae to be internalized into the "caveosomes" under a neutral condition (30). In contrast, effective internalization of SV40 was also found in cells that do not express caveolin-1, suggesting that SV40 utilizes not only the caveola-dependent pathway but also the lipid-raft-dependent and caveola-independent pathway (6). Other viruses utilizing the caveola-dependent pathway include some of the picornaviruses (21), papillomaviruses (4), filoviruses (8), and retroviruses (2).

The binding and subsequent entry of SARS-CoV into the host cells are primarily mediated by a viral spike glycoprotein, called S protein, which binds to its receptor, angiotensin-converting enzyme 2 (ACE2) (16). ACE2 is a cell-surface-bound enzyme of the type I membrane protein topology, with its

* Corresponding author. Mailing address: Department of Microbiology and Immunology, Tohoku University Graduate School of Medicine, 2-1 Seiryo-machi, Sendai, 980-8575 Japan. Phone: 81-22-717-8096. Fax: 81-22-717-8097. E-mail: n-tanaka@mail.tains.tohoku.ac.jp.

▽ Published ahead of print on 23 May 2007.

catalytic site exposed to the extracellular surface. ACE2 along with its related family protein ACE is indispensable for blood pressure homeostasis via the renin-angiotensin system (31). However, despite the 40% amino acid identity shared by ACE and ACE2, ACE does not act as a SARS-CoV receptor (25). The broad expression profile of ACE2, which includes the gastrointestinal tract and lungs, matches well with the affected organs in patients with SARS (9). Although accumulating evidence has documented a physical and functional interaction between SARS-CoV and ACE2, little is known about how the ACE2-mediated entry of SARS-CoV is linked to cellular endocytosis machineries.

In the present study, we investigated the internalization mechanisms of SARS-CoV after binding to ACE2. We found that SARS-CoV hijacks the clathrin-dependent machinery for endocytosis via ACE2 with the cytoplasmic tail deleted, as well as the wild-type ACE2.

MATERIALS AND METHODS

Cell lines. The cell lines used here were human hepatoma HepG2 and monkey kidney COS7 cell lines, which were maintained in Dulbecco modified Eagle medium supplemented with 10% fetal calf serum (FCS) and antibiotics, under 5% CO_2 in a humidified incubator.

Virus and infection. SARS-CoV (Vietnam/NB-04/2003) was maintained in Vero E6 cell cultures as described previously (43). In brief, the SARS-CoV titer of the stock virus was determined by infection of Vero E6 cells by a 50% tissue culture infective dose. Cells were inoculated by SARS-CoV at a multiplicity of infection of 1 and allowed to adsorb the virus for 1 h at 4°C. Subsequently, the cells were washed with phosphate-buffered saline (PBS) and cultured for the indicated times. All experiments using infectious SARS-CoV was done in a laboratory certified with biosafety level 3.

RNA extraction and RT-PCR. Total RNA from HepG2 cells infected with SARS-CoV was extracted with the TRIzol reagent (Invitrogen Corp.) by the following the protocol. Reverse transcription-PCR (RT-PCR) for the detection of viral RNA was performed with Titan One-Tube RT-PCR kit (Roche Molecular Systems) by following the manufacturer's protocol. The primer sequences for SARS-CoV detection were gained from World Health Organization network laboratories. The sequence of BNIoutS2 (sense) is 5′-ATGAATTACCAAGTCAATGGTTAC-3′, and the sequence of BNoutAs (antisense) is 5′-CATAACCAGTCGGTACAGCT AC-3′. For an internal control, a primer set of GAPDH (glyceraldehyde-3-phosphate dehydrogenase) was used. The sequence of GAPDH-F (sense) is 5′-AGTC AGCCGCATCTTCTTTTGC-3′, and the sequence of GAPDH-R (antisense) is 5′-CTCCTGGAAGATGGTGATGGGA-3′.

Pseudoviruses. The pseudoviruses were SARS-CoV(HIV), VSV(HIV), and A-MLV (amphotropic murine leukemia virus)(HIV), which consist of the viruses' respective envelope glycoprotein, the HIV Gag/Pol proteins, and a luciferase plasmid. The pseudoviruses were produced with methods described previously (41). In brief, 293T cells were transfected with 7 μg of pCMVΔR8.1 (HIV Gag/Pol plasmid) and 7 μg of pHR′-luciferase, along with an expression vector for the respective viral envelope glycoprotein: 800 ng of pCMV-SARS-S (SARS-CoV S plasmid), 7 μg of pMD.G (VSV G plasmid), or 7 μg of pDJ (A-MLV envelope glycoprotein plasmid). The 293T cells were cultured in 10-cm dishes, and transfection was performed by the calcium phosphate method. At 48 h posttransfection, the culture supernatants were harvested and filtered through 0.45-μm-pore-size screens. These filtered supernatants were used to infect host cells with the pseudoviruses.

Preparation of ACE2 mutants. Three mutants of ACE2 were prepared from pcDNA ACE2 expression vector (20). ACE2-Δtail mutant has a stop codon at the end of the transmembrane domain, ACE2-Δtail-TM mutant is ACE2-Δtail mutant replaced with the transmembrane domain derived from EGFR, and ACE2-sol consists of the extracellular domain of ACE2. The extracellular domains of ACE2-sol from pcDNA ACE2 were amplified by PCR and introduced into pCXN2 after XhoI digestion. These plasmids were transfected with FuGeneHD according to the manufacturer's instructions (Roche Molecular Systems).

Luciferase assay. Cells were infected with pseudovirus for 12 h, and the culture medium was then replaced with virus-free Dulbecco modified Eagle medium. After further 48 h of incubation, the cells were lysed for luciferase assays. The Dual-Luciferase Reporter Assay System (Promega) was used according to the manufacturer's protocol. The luciferase activities of the samples were measured with a Lumat LB 9507 (Berthold).

Inhibition of endocytosis and endosomal acidification. Extraction of cholesterol from the plasma membranes was performed by using methyl-β-cyclodextrin (MBCD; Sigma), as described elsewhere (7). HepG2 cells seeded in a 24- or a 96-well plate 1 day prior to the experiments were treated with serially diluted MBCD for 30 min. After extensive washes with ice-cold PBS, pseudoviruses were added in the absence of MBCD for an additional 12 h. For the inhibition of clathrin-mediated endocytosis, cells were incubated with the respective doses of chlorpromazine (Sigma) for 1 h and then infected with the pseudovirus for an additional 12 h in the presence of chlorpromazine. After extensive washes with PBS, cells were further incubated in the absence of chlorpromazine for 48 h. To determine the pH dependency of the pseudoviruses, the cells were pretreated with serial dilutions of an endosome acidification inhibitor, either NH_4Cl (Sigma) for 1 h, and then infected with pseudoviruses in the presence of the inhibitor. Luciferase activities were determined for cell extracts prepared from these cultures 48 h after the infection.

Immunoblotting. Immunoblotting assays were performed as described previously (17). In brief, cells were lysed in NP-40 lysis buffer (1% Nonidet P-40, 40 mM Tris-HCl [pH 7.5], 150 mM NaCl, 2 mM EDTA, 1 mM phenylmethylsulfonyl fluoride, and 20 μg of aprotinin/ml). The cell lysates were precleared of cellular debris by centrifugation (10,000 × g) for 30 min at 4°C and subjected to sodium dodecyl sulfate-polyacrylamide gel electrophoresis, and the proteins were electrotransferred onto polyvinylidene difluoride membranes (Millipore). The membranes were first blocked with 5%% nonfat milk in Tris-buffered saline containing 0.1% Tween 20 and then probed with the indicated primary antibodies. The antibodies used were anti-human CHC (Santa Cruz), anti-α-tubulin (Sigma), and anti-ACE2 (R&D Systems). After three washes, the membranes were probed with horseradish peroxidase-conjugated secondary antibodies (Cell Signaling Technology). Signals were visualized with a Super Signal Pico Detection kit (Pierce), and digital images were collected with a Lumi-Imager F1 (Roche Molecular Systems).

Depletion of CHC by siRNA. To transfect small interfering RNA (siRNA) designed to target the clathrin heavy-chain gene (Invitrogen Corp.), a reverse transfection method was used by using Lipofectamine RNAiMAX (Invitrogen Corp.) according to the manufacturer's instructions. In brief, 5 pmol of stealth siRNA duplex-Lipofectamine RNAiMAX complexes were used for 10^5 HepG2 cells in a 24-well plate. Gene silencing efficiency was assessed 48 h after the transfection by immunoblotting. The siRNA (clathrin heavy chain [CHC]) target sequence was 5′-UGAAGUAUUGACAUCAAAUUUCCGG-3′. A nonfunctional oligonucleotide was used for the control (Invitrogen Corp.).

Immunofluorescence staining. HepG2 cells were grown in 35-mm glass-bottom dishes (Iwaki) at a density of 4×10^4 cells/dish. After 24 h, the cells were washed twice with PBS, fixed with 4%% paraformaldehyde for 15 min, washed with the wash buffer (0.1% Triton X-100–PBS), and blocked with the same buffer containing 10% FCS. For immunostaining, samples were incubated overnight with the primary antibodies, including anti-ACE2 and anti-EEA1 (Santa Cruz). After three washes, the samples were incubated with the secondary antibodies (Molecular Probes; Alexa 488-labeled and Alexa 594-labeled antibodies) for 1 h. Confocal imaging was performed by using the 510 META microscope with a 60×/1.30-0.60 oil immersion objective lens (Carl Zeiss).

RESULTS

Effects of endocytosis inhibitors on SARS-CoV entry. To investigate the entry mechanism of SARS-CoV, we used SARS-CoV(HIV), because it allows safe, rapid, and quantitative analyses. Two other pseudoviruses, the VSV(HIV) and A-MLV(HIV), were used as control viruses, because VSV(HIV) utilizes the pH-dependent and clathrin-dependent entry mechanisms (40), while A-MLV(HIV) utilizes the pH-independent and clathrin-independent entry mechanisms (2, 25, 40).

HepG2 cells were infected with pseudoviruses, SARS-CoV-(HIV), VSV(HIV), or A-MLV(HIV) in the presence of an endocytosis inhibitor, chlorpromazine. Chlorpromazine is a cationic amphiphilic drug that disrupts clathrin-mediated endocytosis by inhibiting the relocation of clathrin and AP2 from the cell surface (42). HepG2 cells were pretreated with various

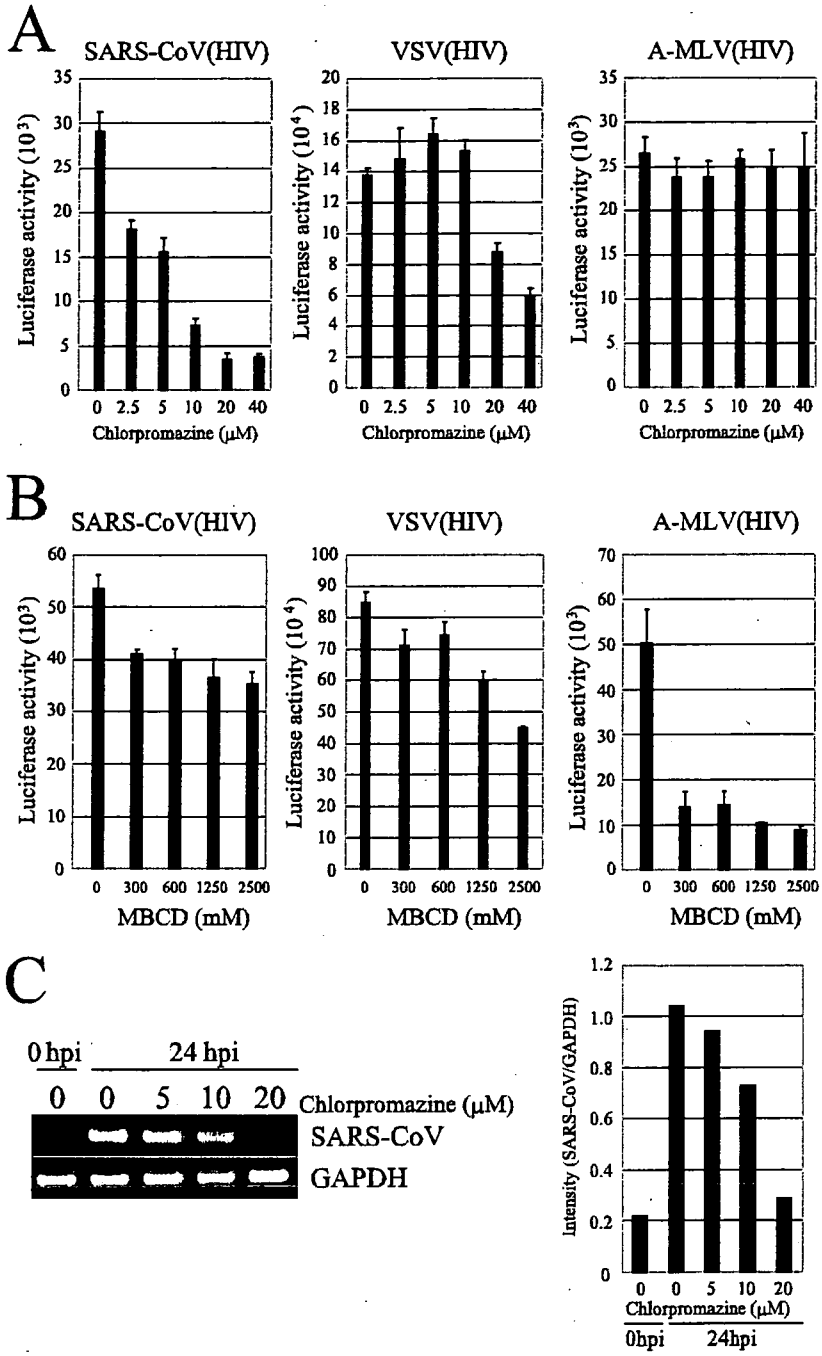

FIG. 1. Effects of chlorpromazine and MBCD on pseudoviruses and SARS-CoV infection. (A and B) HepG2 cells were treated with the indicated doses of chlorpromazine or MBCD and then infected with SARS-CoV(HIV), VSV(HIV), or A-MLV(HIV) for overnight. The effects of chlorpromazine and MBCD on the infectivity of each pseudovirus were evaluated by measuring the luciferase activities. The columns represent the mean values of triplicate experiments; bars indicate maximum values. (C) HepG2 cells treated with the indicated doses of chlorpromazine were infected with SARS-CoV (Vietnam/NB-04/2003) for 24 h, and their expressions of viral RNA were measured by RT-PCR.

doses of chlorpromazine for 1 h and then infected with the indicated pseudovirus in the presence of chlorpromazine (Fig. 1A). Chlorpromazine significantly inhibited the infection efficiency of SARS-CoV(HIV); only 14% infectivity was observed with 20 μM chlorpromazine. Infection by VSV(HIV) was also inhibited, but less so; 42% infectivity was still seen with 20 μM chlorpromazine. Unlike the other two pseudoviruses, infection by A-MLV(HIV) was largely unaffected by any concentration of chlorpromazine.

We also examined the effects of another endocytosis inhibitor, MBCD, on infections by the pseudoviruses, because MBCD disrupts cholesterol-rich microdomains, resulting in

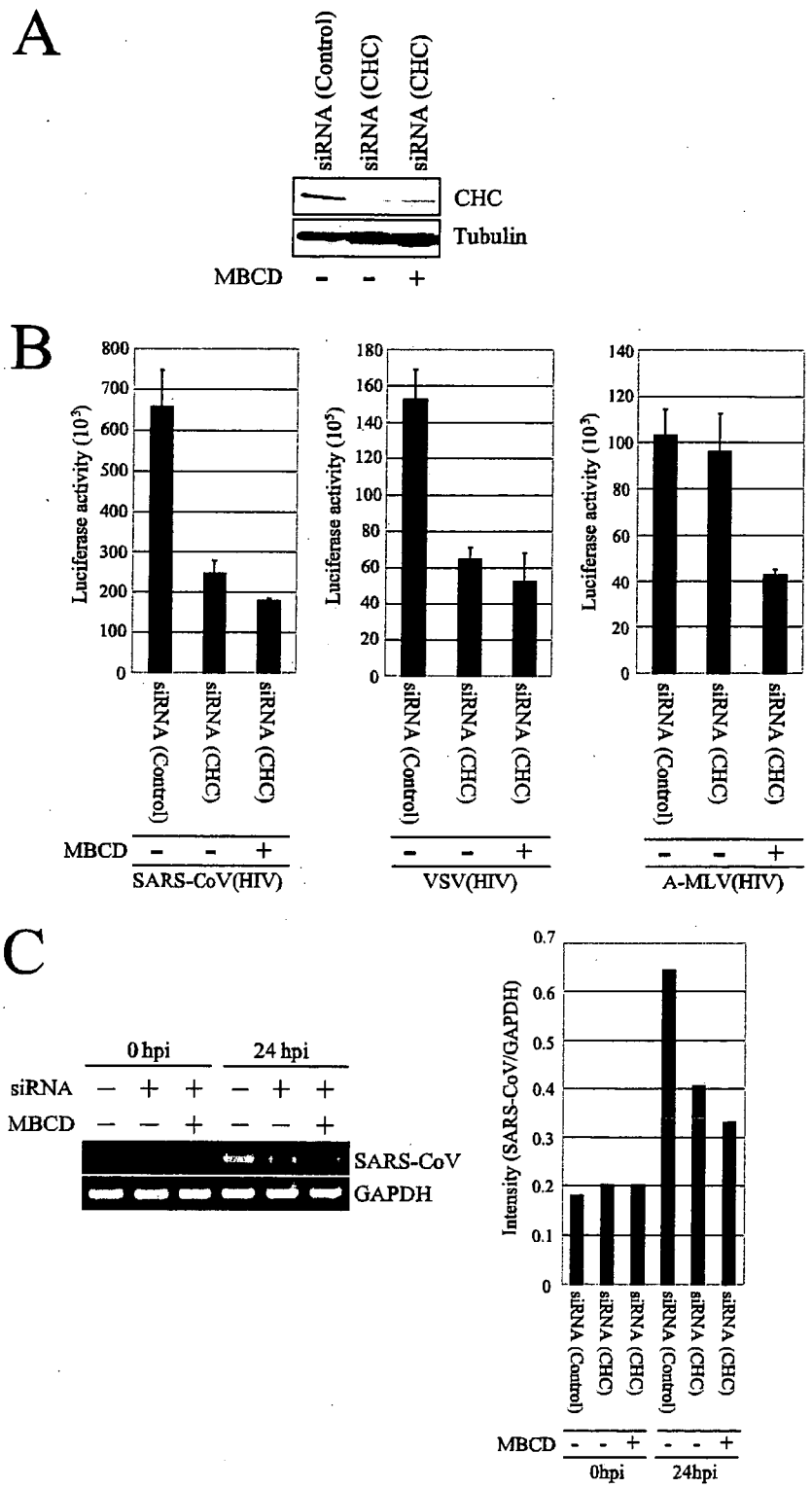

FIG. 2. Effects of CHC-specific siRNA on pseudoviruses and SARS-CoV infection. (A) HepG2 cells were transfected with the CHC-specific siRNA or the control siRNA and analyzed by immunoblotting with anti-CHC or anti-tubulin monoclonal antibody after 48 h of transfection. (B) The cells were treated with 2.5 mM MBCD for 30 min and then infected with each pseudovirus. The infectivities of the pseudoviruses are represented as luciferase activities. The experiment was performed in triplicate. (C) The cells were also infected with SARS-CoV (Vietnam/NB-04/2003) for 24 h, and their expressions of viral RNA were measured by RT-PCR.